Interhemispheric reactivity of the subthalamic nucleus sustains progressive dopamine neuron loss in asymmetrical parkinsonism

Pascal Salin, Christophe Melon, Carine Chassain, Guilhem Pages, Bruno Pereira, Yann Le Fur, Franck Durif, Paolo Gubellini, Lydia Kerkerian-Le goff

Neurobiology of Disease 191 (2024) 106398

Contents lists available at ScienceDirect

Neurobiology of Disease

journal homepage: www.elsevier.com/locate/ynbdi

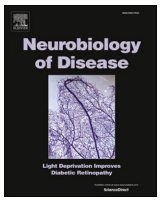

Interhemispheric reactivity of the subthalamic nucleus sustains progressive dopamine neuron loss in asymmetrical parkinsonism

Pascal Salin [a,1], Christophe Melon [a,1], Carine Chassain [b,c,1], Paolo Gubellini [a,1,2], Guilhem Pages [c,d], Bruno Pereira [e], Yann Le Fur [f], Franck Durif [b,*], Lydia Kerkerian-Le Goff [a,*]

[a] Aix-Marseille Univ, CNRS, IBDM, Marseille, France
[b] University of Clermont Auvergne, CHU, CNRS, Clermont Auvergne INP, Institut Pascal, F-63000 Clermont-Ferrand, France
[c] INRAE, AgroResonance Facility, F-63122 Saint-Genès-Champanelle, France
[d] INRAE, UR QuaPA, F-63122 Saint-Genès-Champanelle, France
[e] University Hospital Clermont-Ferrand, Biostatisticis Unit (DRCI), Clermont-Ferrand, France
[f] Aix-Marseille Univ, CNRS, CRMBM, Marseille, France

ARTICLE INFO

Keywords:
Corticostriatal
Glutamate
Interhemispheric
Metabolic changes
^{1}H-magnetic resonance spectroscopy
Nigrostriatal
Parkinson's disease
Subthalamic nucleus
Slice electrophysiology
Neuroprotection

ABSTRACT

Parkinson's disease (PD) is characterized by the progressive and asymmetrical degeneration of the nigrostriatal dopamine neurons and the unilateral presentation of the motor symptoms at onset, contralateral to the most impaired hemisphere. We previously developed a rat PD model that mimics these typical features, based on unilateral injection of a substrate inhibitor of excitatory amino acid transporters, L-trans-pyrrolidine-2,4-dicarboxylate (PDC), in the substantia nigra (SN). Here, we used this progressive model in a multilevel study (behavioral testing, in vivo ^{1}H-magnetic resonance spectroscopy, slice electrophysiology, immunocytochemistry and in situ hybridization) to characterize the functional changes occurring in the cortico-basal ganglia-cortical network in an evolving asymmetrical neurodegeneration context and their possible contribution to the cell death progression. We focused on the corticostriatal input and the subthalamic nucleus (STN), two glutamate components with major implications in PD pathophysiology. In the striatum, glutamate and glutamine levels increased from presymptomatic stages in the PDC-injected hemisphere only, which also showed enhanced glutamatergic transmission and loss of plasticity at corticostriatal synapses assessed at symptomatic stage. Surprisingly, the contralateral STN showed earlier and stronger reactivity than the ipsilateral side (increased intraneuronal cytochrome oxidase subunit I mRNA levels; enhanced glutamate and glutamine concentrations). Moreover, its lesion at early presymptomatic stage halted the ongoing neurodegeneration in the PDC-injected SN and prevented the expression of motor asymmetry. These findings reveal the existence of endogenous interhemispheric processes linking the primary injured SN and the contralateral STN that could sustain progressive dopamine neuron loss, opening new perspectives for disease-modifying treatment of PD.

1. Introduction

Parkinson's disease (PD) is the second most common neurodegenerative disorder. Its main pathological hallmarks are the progressive loss of nigrostriatal dopamine neurons and the presence of Lewy body inclusions, constituted by the deposition of misfolded proteins among which α-synuclein is a major component (Dauer and Przedborski, 2003). A cascade of multifactorial pathogenic events, including protein misfolding, failure of degradation systems (ubiquitin proteasome pathway and autophagy), mitochondrial dysfunction, neuroinflammation, oxidative stress and excitotoxicity, sustains the degenerative process (Cheung and Ip, 2009; Dauer and Przedborski, 2003; Michel et al., 2016; Olanow, 2007; Schapira and Jenner, 2011). Among these factors, increasing experimental evidence links PD-like neurodegeneration with defective function, expression or trafficking of excitatory amino acid transporters (EAATs) (Aoyama et al., 2008; Assous et al., 2014; Berman et al., 2011; Iovino et al., 2022; Nafia et al., 2008; Zhang et al., 2020; Zhang et al., 2016). EAATs not only ensure the bulk of extracellular

* Corresponding authors.
E-mail addresses: franck.durif@uca.fr (F. Durif), lydia.kerkerian-le-goff@univ-amu.fr (L. Kerkerian-Le Goff).
[1] These authors contributed equally to this work.
[2] Present address: Aix-Marseille Univ, CNRS, LNC, Marseille, France.

https://doi.org/10.1016/j.nbd.2023.106398
Received 30 October 2023; Received in revised form 21 December 2023; Accepted 30 December 2023
Available online 3 January 2024

glutamate (Glu) clearance but also fuel essential intracellular metabolic pathways, such as the synthesis of glutathione. Therefore, defaults in their function might sustain both excitotoxicity and reduced antioxidant defense (see (Had-Aissouni, 2012; Li et al., 2021; Magi et al., 2019)).

An intriguing feature of PD is that the cardinal motor symptoms have an asymmetric presentation in most cases (Barrett et al., 2011; Djaldetti et al., 2006; Pagano et al., 2016). For a majority of patients, they emerge as unilateral and spread to the other body side with the disease progression while worsening in the initially affected side, so that the asymmetry remains detectable at advanced stages. Symptom dominance has been related to handedness, and the type and side of motor sign onset have been linked to the progression of both the motor and the non-motor symptoms (Riederer et al., 2018; Schapira et al., 2017; Uitti et al., 2005; van der Hoorn et al., 2012). From a pathological point of view, this clinical lateralization has been associated with an asymmetry of the damage/dysfunction of the substantia nigra (SN) and the putamen (Choe et al., 1998; Prasad et al., 2018), more particularly of the alterations in dopaminergic markers (Bohnen et al., 2006; Huang et al., 2001; Marek et al., 1996; Wang et al., 2015; Yagi et al., 2010), and has also a cortical signature (Claassen et al., 2016). These alterations predominate contralateral to the side of motor symptom onset. Noteworthy, it has been reported that healthy subjects have symmetric nigrostriatal dopaminergic function (Garrido et al., 2020) and that motor symptoms and striatal dopaminergic denervation are more symmetric in patients with Lewy body dementia compared to PD (Fedorova et al., 2023). The mechanisms underlying the pathological asymmetry in PD are not fully understood. They presumably involve genetic and environmental determinants (Riederer et al., 2018; Wiberg et al., 2019), including hemispheric differences in neuronal epigenomes (Li et al., 2020), which may affect the progression and symptoms of PD. Peculiarities of the pathogenic process might also have a role, as proposed in the α-Synuclein Origin site and Connectome model (SOC model) (Borghammer, 2021), which assumes that the initial location of α-synuclein pathological seeds (brain-first vs. body-first) and connection-dependent propagation of the pathology determines the asymmetry/symmetry of the degenerative process in Lewy body pathologies.

Most of our knowledge on the pathophysiology of PD comes from animal models that do not reproduce the progressive character and asymmetrical evolution of the neurodegenerative process characterizing PD (Blesa and Przedborski, 2014; Gubellini and Kachidian, 2015). Interestingly, among the models showing progressive neurodegeneration, some present a unilateral to bilateral evolution of the dopamine neuron loss, pointing to the involvement of interhemispheric mechanisms in the cell death progression. They include rats with unilateral injection of the substrate inhibitor of EAATs L-trans-pyrrolidine-2,4-dicarboxylate (PDC) in the SN (Assous et al., 2014) or of α-synuclein preformed fibrils in the striatum (Patterson et al., 2019). In the two studies, sensorimotor deficits emerge when the loss of SN dopaminergic neurons in the injected brain side reaches 50 to 60% and, similarly, contralateral degeneration occurs after a threshold of ipsilateral degeneration has been met. Hence, these models mimic the unilateral presentation of symptoms associated with progressive asymmetrical damage to the nigrostriatal system. They may thus be useful both for addressing the pathophysiology of early PD in an evolving neurodegeneration context and for elucidating pathological mechanisms that might contribute to the progression of the neurodegenerative process. The substrates of the unusual degeneration phenotype in the PDC model remain unknown. Although the cell-to-cell spread of α-synuclein pathology provides a potential basis for cell death evolution in models of synucleopathies, the lack of inclusions in the contralateral SN in the study by Patterson et al. led to suggest an additional mechanism affecting the contralateral hemisphere. In the two papers, a similar scenario has been proposed in which interhemispheric imbalance produced by the initial unilateral insult induces a cascade of adaptive changes resulting in an overactivity of glutamatergic inputs to the contralateral SN and subsequent excitotoxicity. Here, we used the progressive PDC-based model of parkinsonism and a combination of in vivo and ex-vivo approaches to characterize the reactivity of glutamatergic components of the cortico-basal ganglia network. We focused on the corticostriatal pathway and the subthalamic nucleus (STN), whose abnormal activation is central in the pathophysiology of PD and is suggested to contribute to nigrostriatal neurodegeneration via α-synuclein-mediated mechanisms and excitotoxicity (Blandini et al., 1996; Finlay and Duty, 2014; Foffani and Obeso, 2018; Muddapu et al., 2019; Rodriguez et al., 1998). As main findings, we evidence an early and persistent reactivity of the STN contralateral to the primary injury, and show that its lesion at early presymptomatic stage prevents the late expression of motor deficits and halts the progression of the degeneration in the PDC-injected SN. These results reveal the implication of complex interhemispheric adaptive mechanisms involving the STN in a model of progressive asymmetrical PD, with potential relevance for the development of disease-modifying strategies.

2. Materials and methods

2.1. Animals and experimental layout

Experimental procedures were carried out in accordance with EU Directive 2010/63/EU for the care and use of Laboratory animals. They have been approved by the local and national Ethical Committees (project authorization delivered by the French Ministry of Higher Education, Research and Innovation: #8616-2017011918055786v5). Male Wistar Han rats (Charles River, France) were utilized, housed 4 per cage (Type IV cages, 1500 cm2) at 21 ± 1 °C in a light controlled environment (12 h light/dark cycle) with access to food and water ad libitum (except during deprivation for behavioral tests, see below). Experimental groups are defined as follows: sham (animals with unilateral vehicle injection in the left SN); PDC (rats receiving PDC injection in the left SN); PDC + ibot (rats submitted to PDC injection in the left SN and, 7 days later, to contralateral STN lesion by local ibotenic acid injection). The time of vehicle or PDC injection in the SN is defined as time 0, while the other points are “days post-injection” (dpi). Different subsets of sham and PDC animals were used for the following experiments: longitudinal behavioral assessment followed by proton magnetic resonance spectroscopic imaging (^{1}H-MRSI) (repeated measures at 30, 60 and 120 dpi), slice electrophysiology (at 120 dpi) and quantitative in situ hybridization (separated subgroups at 4, 30 and 120 dpi). All groups were processed for quantitative analysis of nigral dopamine neuron loss using tyrosine hydroxylase (TH) immunodetection at the ending point of each experiment (Fig. 1A). Animals of the PDC + ibot experiment underwent behavioral testing followed by ^{1}H-MRSI at 120 dpi and were thereafter processed for both TH immunodetection and histological control of the STN lesion (Fig. 1B). The criteria for animal exclusion from the analyses were: incorrect STN lesion for the PDC + ibot group; one time point missed for technical reasons in an individual that underwent repeated assessments (longitudinal behavioral and ^{1}H-MRSI study). No sample from the selected animals (given as n in the figure legends) was discarded.

2.2. Surgical procedures

Intranigral stereotactic injection of PDC was performed in groups of 7–8 weeks old rats (180–200 g), as previously reported (Assous et al., 2014). Animals under equithesin anesthesia (4 ml/kg) were mounted in a stereotactic apparatus (Kopf Instruments) and received injection of 300 nmol PDC (5 µl of a 60 mM PDC solution at the rate of 1 µl/min) or vehicle (0.9% NaCl; 5 µl at the rate of 1 µl/min) in the left SN (coordinates in mm: AP +2.2, L ± 2.0, and DV +3.3 versus interaural, according to the atlas by de Groot (De Groot, 1959)). A subset of the PDC animals received injection of ibotenic acid (7.6 µg/0.8 µl at a rate of 0.2 µl/min) in the right STN, i.e. the STN contralateral to the PDC-injected

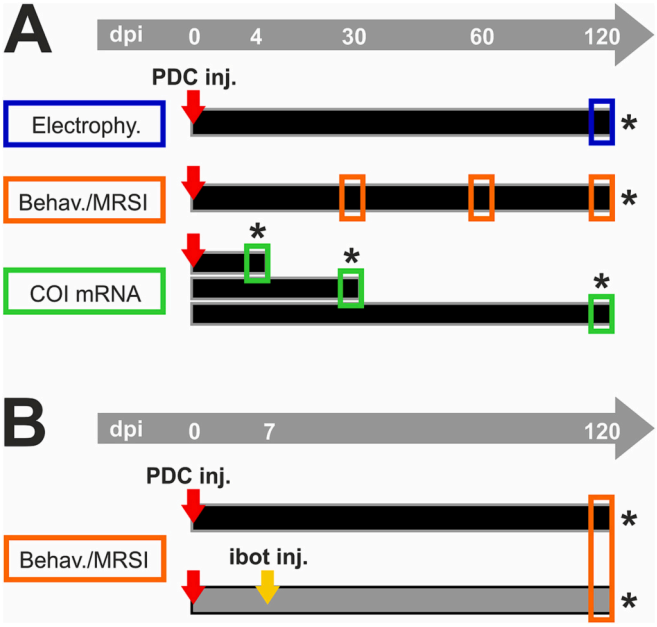

Fig. 1. Experimental plans.
(A) Experimental design and time course of the experiments shown in Figs. 2 to 5. Three groups of rats were unilaterally injected with PDC in the SNc at day 0 (red arrows). Colored boxes show when experiments were performed; asterisks indicate the time points at which brains were processed for TH immunostaining. The "Electrophy." group was utilized for slice electrophysiology at 120 dpi (blue box). The "Behav./MRSI" group underwent three sessions of behavioral testing and ^{1}H-MRSI at 30, 60 and 120 dpi (orange boxes). The "COI mRNA" group consisted in three subgroups that were sacrificed at 4, 30 and 120 dpi for COI mRNA measurements (green boxes). Each experiment included a corresponding group of sham-injected animals that underwent the same experimental procedures (not shown).
B) Experimental layout and time course of the experiments shown in Fig. 6. Two groups of rats received a unilateral intranigral injection of PDC at day 0 (red arrows), and one of them was also injected with ibotenic acid in the contralateral STN at 7 dpi (yellow arrow). Both groups underwent behavioral testing and ^{1}H-MRSI at 120 dpi (orange box), then they were processed for TH immunostaining and histological control of STN lesion (asterisk). A sham group with saline injection in the SNc underwent the same experimental procedures (not shown). (For interpretation of the references to colour in this figure legend, the reader is referred to the web version of this article.)

SN, at 7 dpi. This time point was selected based on our previous work showing modest but significant loss of dopamine neurons of around 20% in the PDC-injected SN pars compacta (SNc) as soon as 4 dpi, which then progressively evolves overtime, but no cell loss in the contralateral SNc. The stereotaxic coordinates for targeting the STN in our animals were in mm: AP – 3.3, L – 2.4 and DV – 7.6, versus Bregma, which correspond to AP – 3.8, L – 2.4 and DV – 8, according to the atlas of (Paxinos and Watson, 1998).

2.3. Behavioral testing

The cylinder test was used to evaluate the motor asymmetry associated with asymmetrical loss of nigrostriatal dopamine neurons. The test was performed repeatedly at 30, 60 and 120 dpi. Animals were placed in a Plexiglas® cylinder (30 cm diameter) and video recorded during 15 min. Forelimb contacts on the cylinder wall while rearing were counted, scoring separately those made using the left (ipsilateral to SN injection), the right (contralateral to SN injection) or both forepaws (double contacts). Results are expressed as an asymmetry score, defined as the percent of contralateral contacts minus the percent of ipsilateral contacts, these percentages being calculated over the total number of contacts (left, right and double). Sham rats are expected to show a score close to zero, reflecting indifferent use of either forepaw, while PDC animals are expected to show a negative asymmetry score due to dopamine neuron loss in the primary injured side over a threshold triggering akinesia-like deficit of the contralateral paw.

2.4. In vivo ^{1}H-MRSI

All imaging experiments were performed at the In Vivo Imaging Auvergne facility (IVIA, Clermont-Ferrand, France; https://doi.org/10.18145/ivia) on a 11.7 T Bruker BioSpec Ultra Shielded Refrigerated system (Bruker BioSpin, Ettlingen, Germany) equipped with a 72-mm ^{1}H circular polarizer volume coil and a rat brain surface coil used for emission and reception, respectively. Animals under inhaled gas anesthesia (1–2.4% isoflurane and air, 300 ml/min) were secured to a handling system. Respiratory rate was monitored all along the session to adjust anesthesia and body temperature was maintained at 37 °C using a warm air system. The rat head was manually positioned at the magnet magnetic center and then localization imaging was performed to validate the position. Multi-slice coronal and axial T2 weighted images were acquired using multi-slice RARE (Rapid Acquisition with Refocusing Echoes) protocols to image the whole brain. Main parameters were: 15.7 ms echo time; 2500 ms repetition time; RARE factor = 4; 2 averages; field of view (FOV) 35 × 35 mm with 256 × 256 points and slice thickness of 1 mm. Acquired images were used to determine on which slices ^{1}H-MRSI was performed.

Two standard coronal 2D ^{1}H MRSI were acquired. One slice was positioned to cover striata while the other one the STNs. ^{1}H-MRSI using a modified CSI (chemical shift imaging) protocol to include semi-LASER (semi-adiabatic localization by adiabatic selective refocusing) volume selection to limit chemical shift artefacts (Meyerspeer et al., 2011). The echo and repetition times were set to 24 and 2000 ms, respectively. To increase the signal to noise ratio, 8 and 16 weighted transients were accumulated for striatal and STN ^{1}H-MRSI, respectively. The FOV was 32 × 32 mm with 20 × 20 points and the slice thickness was 2 mm. The semi-LASER volume selection was done on a FOV of 10 × 10 mm leading to voxel resolution of 1.6 × 1.6 × 2 mm. The signal acquisition contained 2048 points over a bandwidth of 10 ppm leading to an acquisition time of 409.6 ms. Automatic shimming of 1st and 2nd order was performed using MAPSHIM procedure. The water signal was suppressed using a VAPOR (variable power pulses and optimized relaxation delays) scheme with radio frequency pulses having a bandwidth of 350 Hz (Tkac et al., 1999). Striatal and STN ^{1}H-MRSI acquisition times were about 35 and 63 min, respectively. To quantify metabolites, water ^{1}H-MRSI were acquired in the same conditions at the exception of the water suppression pulses, which were not emitted, and only 1 repetition was performed. ^{1}H-MRSI data were processed thanks to the software CSIAPO, which allows grid-free positioning of cylindric regions of interest (Le Fur et al., 2010). Because of the small size of the STN in rat, regions of interest were carefully positioned to cover the whole STN and minimize contamination with surrounding tissues, which mainly correspond to white matter structures (internal capsule, cerebral peduncle). Then spectra from the left and right striata and STN were exported and processed by using LCModel software version 6.3 (Steven Provencher, Oakville, Ontario, Canada) (Provencher, 1993), which uses Bayesian analysis starting with solution spectra basis sets to provide estimates of metabolite and macromolecule concentrations without operator bias. The intensity of the water signal obtained from unsuppressed water spectra was used as an internal reference. Here, we analyzed the levels of glutamatergic transmission-related metabolites, namely Glu and glutamine (Gln), among the neurochemicals that can be measured with this method (see Figs. 4 and 5). For including a quantified metabolite in the group analysis, the output of the LCModel analysis had to (i) measure a half-height line width for the metabolite inferior to 15 Hz, (ii) display a fitting residual line randomly scattered around zero (controlled by visual inspection) and (iii) measure average Cramer–Rao lower bounds (CRLB) calculated by LCModel inferior to 30%. The metabolite

concentrations are determined in mM for each animal and results are expressed as percent of the mean sham value.

2.5. Slice electrophysiology

Brains from 8 PDC-treated rats at 120 dpi and 6 age-related sham were cut in coronal corticostriatal slices (250 μm) by a vibratome (Leica VT1000 S, Germany) in oxygenated ice-cold solution containing (in mM): 110 choline, 2.5 KCl, 1.25 NaH_2PO_4, 7 $MgCl_2$, 0.5 $CaCl_2$, 25 $NaHCO_3$, 7 glucose, 300–310 mOsm, pH 7.4, bubbled with carbogen (95% O_2 and 5% CO_2). Slices were kept in artificial cerebrospinal fluid (ACSF) at room temperature, whose composition was (in mM): 126 NaCl, 2.5 KCl, 1.2 $MgCl_2$, 1.2 NaH_2PO_4, 2.4 $CaCl_2$, 11 glucose, and 25 $NaHCO_3$, 300–310 mOsm, pH 7.4, and also containing 250 μM kynurenic acid and 1 mM sodium pyruvate, bubbled with carbogen. Whole-cell patch-clamp recordings were performed in ACSF (without kynurenic acid and sodium pyruvate) at 35 °C, flowing at ~2.5 ml/min and containing 50 μM picrotoxin (Tocris Bioscience, UK), using borosilicate micropipettes (5–6 MΩ) filled with an internal patch solution containing (in mM): 125 K-gluconate, 10 NaCl, 1 $CaCl_2$, 2 $MgCl_2$, 0.5 1,2-bis (2-aminophenoxy) ethane-N,N,N,N-tetraacetic acid (BAPTA), 19 4-(2-hydroxyethyl)piperazine-1-ethanesulfonic acid (HEPES), 0.3 guanosine triphosphate (GTP), and 1 Mg-adenosine triphosphate (Mg-ATP), pH 7.3, 290–300 mOsm. All recordings were performed in the striatum ipsilateral to intranigral PDC (PDC ipsi) or vehicle injection at 120 dpi. Electrophysiological data were recorded by an AxoPatch 200B amplifier with pClamp 10.2 software (Molecular Devices, USA) at a sampling frequency of 10 kHz. Striatal spiny projection neurons (SPNs) of the dorsolateral striatum were identified by infrared video-microscopy and by their electrophysiological properties (Jiang and North, 1991). The number of recorded SPNs for each experiment is indicated in Fig. 3. A stimulating bipolar electrode was placed in the white matter between the cortex and the striatum to evoke AMPA receptor-mediated excitatory postsynaptic currents (EPSCs). SPNs were clamped at −80 mV, and series and input resistance were continuously monitored by sending 5 mV pulses. EPSC amplitude for monitoring long-term depression (LTD) and long-term potentiation (LTP) was measured on averaged traces (6 per minute) to obtain time-course plots, and to compare this parameter before (baseline) and after the induction protocols. LTD induction protocol consisted in three trains of high-frequency stimulation (100 Hz) of 3 s duration, and with 20 s interval between each train. LTP induction protocol was identical but, during each train, the recorded SPN was depolarized to −10 mV in order to allow strong *N*-methyl-D-aspartate (NMDA) receptor activation (Calabresi et al., 2000a; Calabresi et al., 1992a; Calabresi et al., 1992b; Chassain et al., 2016; Paille et al., 2010; Partridge et al., 2000). EPSC data were analyzed offline by pClamp 10.2 (Molecular Devices, USA). Spontaneous EPSCs (sEPSCs) were recorded for 5 min and analyzed offline by Mini Analysis 6.0.3 (Synaptosoft, USA), using a threshold detection (3–5 pA) that was set at twice the noise of each recording. Only neurons with <20% change in series resistance and stable EPSCs during the whole experiment were considered for the analysis.

2.6. TH immunostaining and cell counting

Animals of the ^{1}H-MRSI and of the PDC + ibot experiments were perfused transcardially with 400 ml 4% PFA in PBS 0.1 M, pH 7.3. Brains were dissected, left 24 h in the same fixative and then transferred in 30% sucrose (2 × 48 h). They were then frozen on dry ice and kept at −80 °C until sectioning. Serial frontal cryosections (40 μm) covering the whole extent of the SNc were collected in PBS. TH fluorescence immunostaining was done on a set of 6 evenly-spaced sections for each animal covering the PDC peri-injection and posterior zone as defined in (Assous et al., 2014). After rinses, sections were immersed in 0.3% Triton X-100 in PBS (2 × 15 min), pre-incubated for 30 min in PBS containing 5% BSA, incubated overnight with mouse anti-TH primary antibody (1:1000, Millipore) then incubated 2 h with secondary fluorescent antibodies (Alexa Fluor goat anti-mouse 568; 1:200). The stained sections were mounted on coverslips with mounting reagent (FluorSave reagent, Calbiochem) and kept away from light until analysis. Quantitative analysis of TH-positive cells was performed as previously detailed (Dinh et al., 2021) using a Zeiss microscope with AxioImager M2 Apotome from the IBDM microscopy platform. Photomicrographs were taken with the ZEN 2 Blue edition Zeiss software. Using ImageJ, SNc was delineated and the nuclear profiles of all immunostained cells were counted to exclude any bias that could result from changes in cell soma size or shape among experimental conditions. The total number of labeled neurons in the SNc region examined (640 μm anteroposterior extent) was estimated for each animal by summing the values obtained in the six sections and multiplying it by a factor of eight to take into account the staining penetration in the depth of the 40 μm section (15 μm as determined with an acquisition in *Z*-stacks) and the sampling (one out of every three serial sections, cumulated thickness 120 μm). This number was then corrected using Abercrombie's correction formula.

For animals of the electrophysiology and of the in situ hybridization experiments, TH immunostaining was performed on coronal cryostat sections at SNc level (16 μm) cut from fresh frozen brain tissue. Sections were collected in PBS and fixed with 4% paraformaldehyde for 10 min before being processed for TH immunodetection as described above. Quantitative analysis was done on a set of 3 sections at peri-injection level per animal as described above and averaged. For all conditions, individual results are expressed in percentage of the mean sham value.

2.7. Nissl staining

Nissl staining using toluidine blue was performed to assess the extent and appropriate location of the STN lesion in the PDC + ibot group. Frontal cryosections (40 μm) at the level of STN were collected in PBS, then mounted on Superfrost™ slides and left to dry overnight. Sections were then sequentially rehydrated in PBS for 10 min, incubated in 0.25% toluidine solution, rinsed twice in PBS, left to dry overnight, immersed twice in absolute alcohol then twice in xylene, and coverslipped with DPX mounting medium (Sigma Aldrich).

2.8. Cytochrome oxidase subunit I mRNA in situ hybridization

Brains were quickly removed, frozen in dry ice and kept at −80 °C until cryostat sectioning. Coronal 16 μm-thick tissue sections at the level of the STN were cut at 20 °C, thaw mounted onto SuperFrost plus glass slides (Fisher Scientific, Elancourt, France) and stored at −80 °C until being processed for radioactive in situ hybridization at cellular level as reported previously (Bacci et al., 2002). In brief, slide-mounted sections were post-fixed for 5 min in 3% PFA and incubated in prehybridization buffer containing 2× standard saline citrate (SSC). The probe was a 44-mer synthetic oligonucleotide DNA complementary to bases 6191–6235 of the rat cytochrome oxidase subunit I (COI) mRNA. This probe was 3′-end-labeled by terminal deoxynucleotide transferase with ^{35}S-dATP (1300 Ci/mmol) using a DNA-tailing kit (NEN), then purified on a mini Quick Spin Oligo Column (Roche, Meylan, France). After prehybridization and dehydration, each section was covered with 35 μl of hybridization buffer containing the probe (500,000 cpm per section) and incubated overnight at 47 °C in humid chamber. After post-hybridization, sections were coated with Amersham LM1 autoradiographic emulsion, exposed at 4 °C for 5 days and developed in Kodak D-19 (4 min at 13 °C), then counterstained with toluidine blue. Sections were observed first under bright-field illumination to point the counterstained neurons, then under dark-field epilumination to measure the number of grains per neuron (final magnification 1000×). Quantitative analysis was done using the Visioscan image analysis software (BIOCOM) on 100 labeled cells per section randomly distributed in the STN for each brain side. The number of silver grains per labeled cell was estimated by measuring OD with respect to a standard curve. This

quantification was performed on 3 sections per animal and the values were averaged. Individual results are expressed as percentage of the mean corresponding sham value.

2.9. Statistical analyses

Statistical analyses were performed using Prism 7 software (GraphPad, USA). All data sets were checked for normal distribution using the Shapiro-Wilk's test; when their distribution met the normality criterion, statistical comparisons were performed by parametric tests, otherwise, non-parametric tests were used. ^{1}H-MRSI data were analyzed by two-way repeated measures ANOVA with groups (sham, ipsi to PDC, contra to PDC) as the between-factor and dpi (30, 60, 120) as the within-factor, followed by the Tukey's test for post-hoc multiple comparisons. Behavioral data were analyzed by two-way repeated measures ANOVA with groups (sham, PDC) as between-factor and dpi (30, 60, 120) as the within-factor, followed by the Sidak's multiple comparisons test for the animals that underwent longitudinal study; when comparing sham, PDC and PDC + ibot groups at the single time point of 120 dpi, we used one-way ANOVA followed by Tukey's test. Electrophysiological data were analyzed by Kruskal-Wallis test followed by Dunn's multiple comparisons test (LTD and LTP), 2-sample Kolmogorov-Smirnov test (sEPSC amplitude and inter-event interval cumulative distributions) or Mann-Whitney test (sEPSC amplitude and frequency mean values). Kruskal-Wallis test followed by Dunn's multiple comparisons test was used for the analysis of COI mRNA levels. For the analysis of TH cell counts, we used Mann-Whitney test when comparing two groups; when comparing more than two data sets, we used Kruskal-Wallis test followed by Dunn's multiple comparisons or one-way ANOVA followed by Sidak's multiple comparisons test. Spearman correlation test was used to assess the relationship between the number of TH-positive neurons and the striatal levels of Glu and Gln. For all analyses, the significance threshold was set at 0.05 and the results are given in the figures' legends.

3. Results

3.1. Time course of the PDC-induced parkinsonian-like behavioral deficit and nigral dopamine neuron loss

Consistent with our previous report (Assous et al., 2014), PDC animals showed a late onset and progressive establishment of the akinesia-like deficit in the cylinder test. The asymmetry score was close to zero at 30 dpi and did not show significant difference vs. sham. It was slightly but significantly increased at 60 dpi and markedly increased at 120 dpi (Fig. 2A). The 30 dpi time point was then considered as asymptomatic stage, the 60 dpi as onset/early-symptomatic stage and the 120 dpi as symptomatic stage.

The extent of the dopamine lesion in the various experimental PDC groups, assessed by quantitative analysis of TH cell loss in the SNc, is shown in Fig. 2B. At 120 dpi, a reproducible and significant median decrease in the number of cells of about 50% (ranging from 46.5 to 55.6%) was measured in the injected SNc and a lower decrease (from 18.8 to 30%), either significant or not, in the uninjected contralateral SNc. The groups used for COI mRNA in situ hybridization further showed that significant dopamine neuron loss occurs in the injected SN as soon as at 4 dpi, in agreement with our previous time course study (Assous et al., 2014).

3.2. Impact of unilateral intranigral PDC injection at striatal level

3.2.1. Corticostriatal transmission and plasticity

Electrophysiological recordings were performed in the striatum ipsilateral to intranigral PDC or vehicle injection at 120 dpi. PDC animals exhibited a loss of both corticostriatal LTD and LTP (Fig. 3A), as well as an increased frequency, but not amplitude, of sEPSC (Fig. 3B). Overall, these data show that partial dopaminergic neurodegeneration

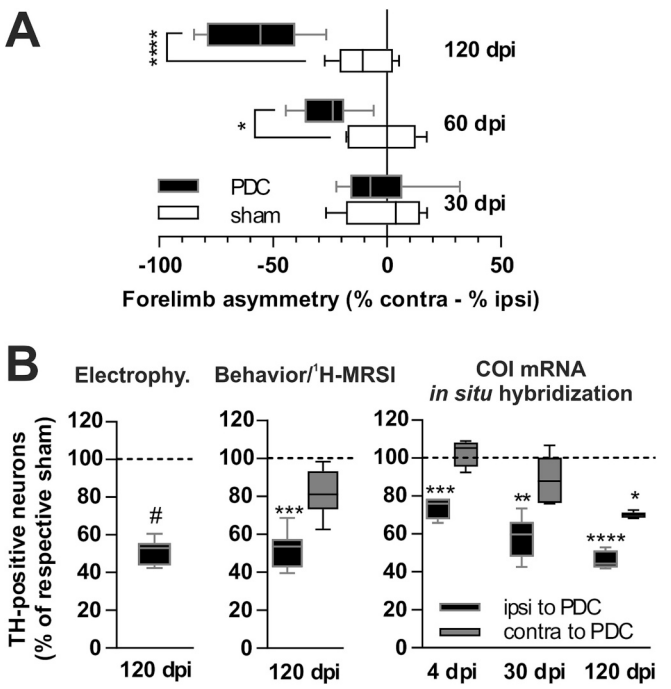

Fig. 2. Behavioral deficit and loss of TH neurons in the PDC-induced model of parkinsonism.
(A) Time-course analysis of unilateral PDC-induced motor deficit in the cylinder test at 30, 60 and 120 dpi. PDC animals show a late onset of akinesia-like deficit as assessed by the asymmetry in forelimb use with modest but significant effect at 60 dpi and a more severe effect at 120 dpi. Sham, $n = 5$; PDC, $n = 8$; two-way repeated measures ANOVA analysis ($F_{group}(1,11) = 14.00$, $P = 0.0033$; $F_{dpi}(2,22) = 14.65$, $P < 0.0001$; $F_{interaction}(2,22) = 7.5$, $P = 0.0033$) followed by Sidak's multiple comparisons test ($^{*}P < 0.05$, $^{****}P < 0.0001$).
(B) Assessment of the loss of TH neurons in the different experimental groups. TH cell loss in the SNc was assessed in the injected SNc for the electrophysiological characterization (Electrophy.) at 120 dpi, in both brain sides for the ^{1}H-MRSI study at 120 dpi, and in both brain sides for the COI in situ hybridization experiment at 4, 30 and 120 dpi. Electrophy.: $n = 3$ sham and 8 PDC, Mann-Whitney test ($^{\#}P < 0.05$ vs. sham). Behavior/^{1}H-MRSI: n = 5 sham and 8 PDC, Kruskal-Wallis ANOVA ($P < 0.0001$) followed by Dunn's multiple comparisons test ($^{***}P < 0.001$ vs. sham). COI mRNA in situ hybridization: $n = 7$ sham and $n = 4$, 6 and 5 PDC at 4, 30 and 120 dpi, respectively; Kruskal-Wallis ANOVA ($P < 0.0001$) followed by Dunn's multiple comparisons post-test ($^{*}P < 0.05$, $^{**}P < 0.01$, $^{***}P < 0.001$ and $^{****}P < 0.0001$ vs. sham).
In **A** and **B**, boxes represent the 25th and 75th percentile (bar = median), whiskers show the min and max values.

resulting from a single unilateral injection of PDC in the SN is sufficient to trigger drastic changes in glutamatergic transmission and plasticity at corticostriatal synapses in the ipsilateral side, similar to those observed after extensive 6-hydroxydopamine lesion (Calabresi et al., 1993; Chassain et al., 2016; Gubellini et al., 2006; Tang et al., 2001).

3.2.2. Glutamate and glutamine levels

^{1}H-MRSI spectra were analyzed in voxels placed in the right and the left striatum of the sham and the PDC rats (Fig. 4A). Metabolic changes were followed at 30, 60 and 120 dpi. Levels of Glu were significantly increased in the striatum ipsilateral to PDC injection at 30, 60 and 120 dpi vs. control values and versus values measured in the contralateral striatum, which did not differ from sham at the three time points examined (Fig. 4B, **left graph**). Levels of Gln were also increased only in the ipsilateral striatum, with significant effect versus sham and contralateral striatum at 30 and 120 dpi (Fig. 4B, **right graph**).

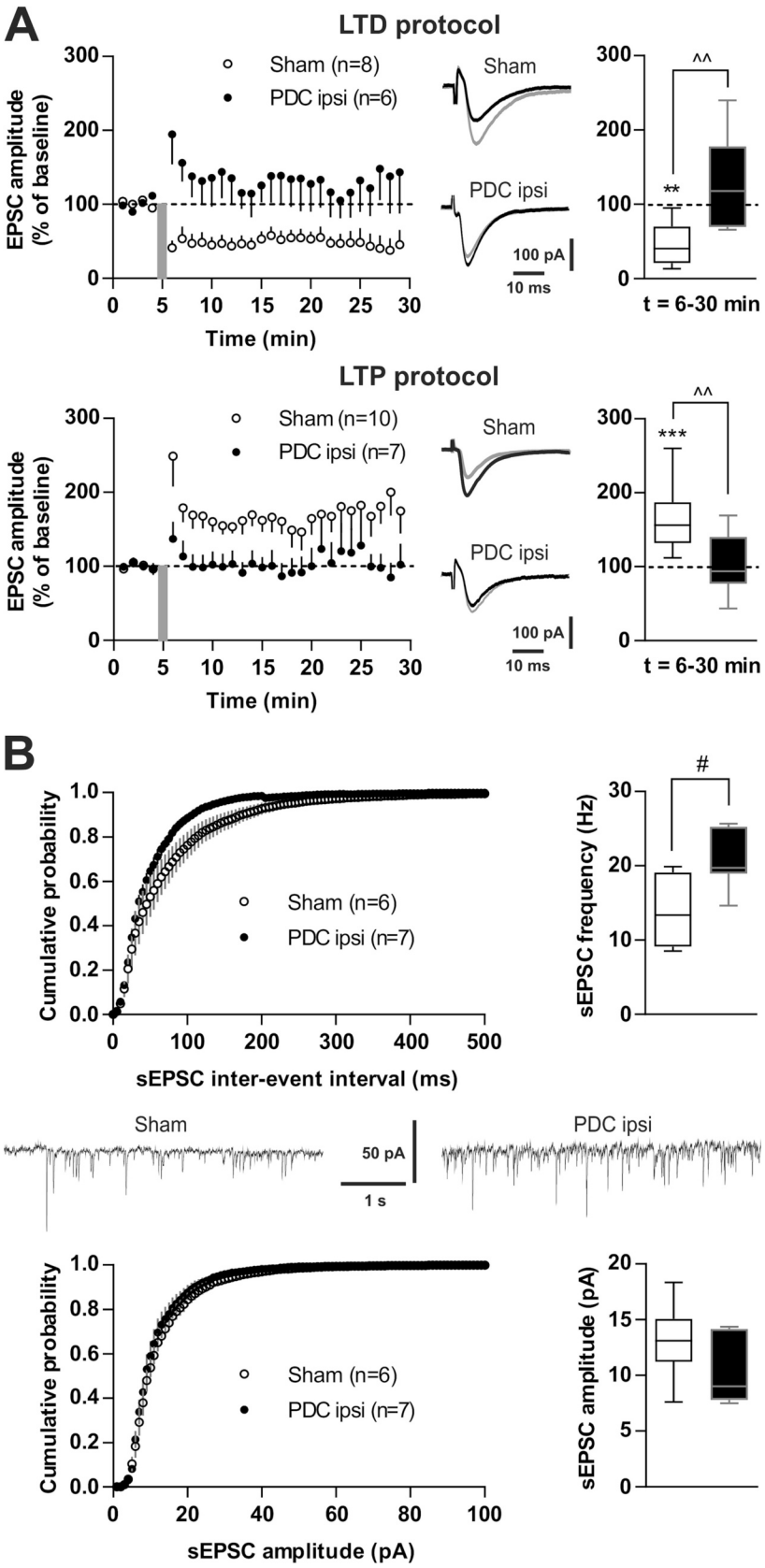

(caption on next page)

Fig. 3. Transmission and plasticity at corticostriatal synapses in unilateral PDC rats.
(A) Corticostriatal LTD (above) and LTP (below) are lost in slices ipsilateral to the intranigral PDC injection at 120 dpi (PDC ipsi), while they are normal in sham. Left graphs depict the time-course of the average EPSC amplitude normalized to the baseline (vertical grey bars represent the induction protocols); right histograms show EPSC amplitude after the induction protocols. Kruskal-Wallis ANOVA ($P = 0.0012$ for LTD and $P = 0.0003$ for LTP) and Dunn's multiple comparisons post-test (***$P < 0.001$ vs. baseline; ^^$P < 0.01$ sham vs. PDC). Traces show sample EPSCs recorded before (grey) and after (black) the induction protocols.
(B) The top graphs show that the sEPSC inter-event interval distribution is shifted to the left (left graph; 2-sample Kolmogorov-Smirnov test: $P < 0.01$) and that the sEPSC frequency is increased in PDC rats compared to sham (right histogram; Mann-Whitney test: $^{\#}P < 0.05$ sham vs. PDC), suggesting that striatal glutamate release is significantly increased. Conversely, the sEPSC amplitude (bottom graphs) is similar in sham and PDC rats, suggesting no change in AMPA receptor sensitivity. In A and B, time-course and cumulative plots values are expressed as mean ± SEM; the number of recorded neurons is indicated in brackets; data were obtained from 8 PDC and 6 sham rats. Boxes represent the 25th and 75th percentile (bar = median), whiskers show the min and max values.

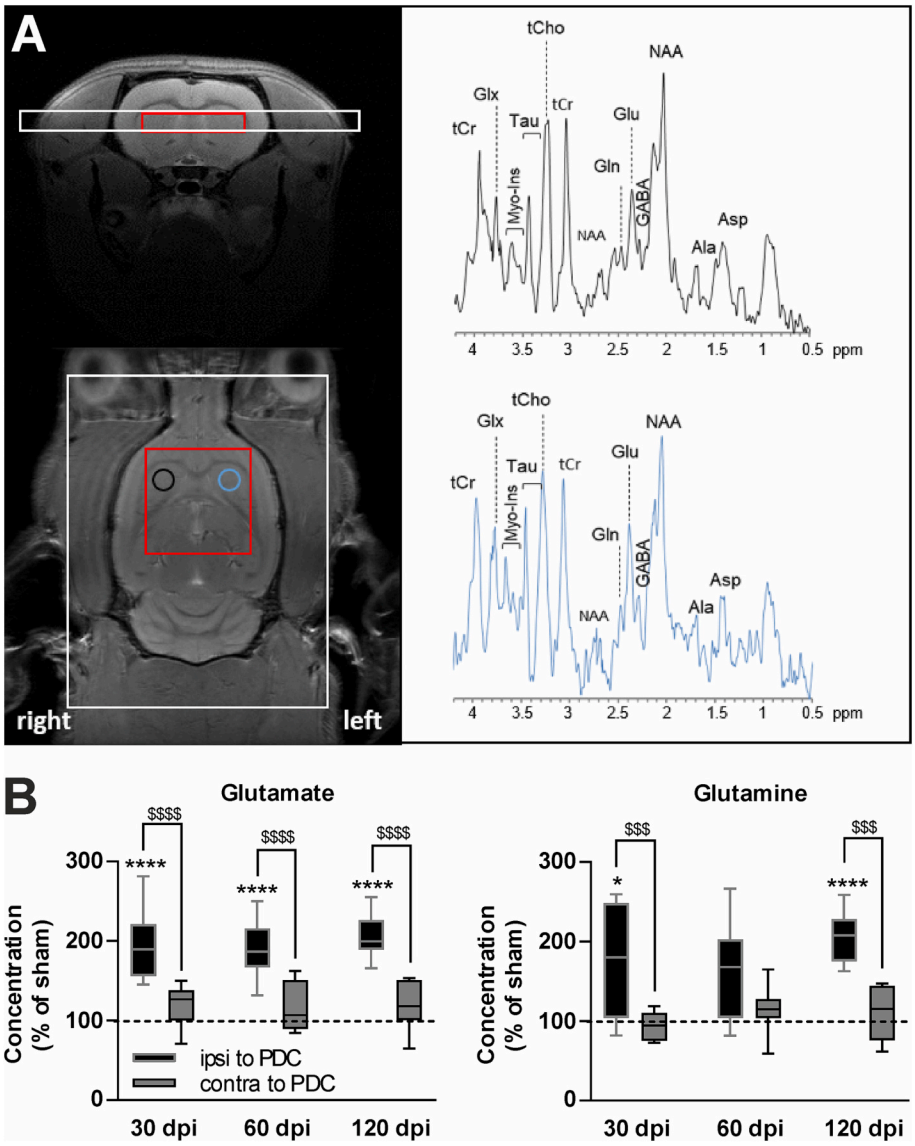

Fig. 4. Measurements of glutamate and glutamine concentrations in the striatum of unilateral PDC rats.
(A) In vivo ^{1}H-MRSI in the striatum. The images on the right are morphological coronal (at the top) and axial (at the bottom) T2-weighted MR images, on which is shown the position of the 2D MRSI grid (red labelling) with the regions of interest covering the striatum of both brain sides. On the left are displayed representative ^{1}H-MRSI spectra obtained in the striatum of the right (black voxel) and the left (blue voxel) hemispheres of a PDC rat, corresponding to the sides contralateral and ipsilateral to PDC injection, respectively. Abbreviations: tCr: total creatine (creatine and phosphocreatine); Myo-Ins: myo-inositol; Tau: taurine; tCho: total choline (glycerophosphocholine and phosphocholine); NAA: *N*-acetylaspartate; Gln: glutamine; Glu: glutamate; GABA: γ-aminobutyric acid; Ala: alanine; Asp: aspartate.
(B) Striatal levels of Glu (left graph) and Gln (right graph) measured at 30, 60 and 120 dpi. The levels of both metabolites are increased vs. sham in the hemisphere ipsilateral to intranigral PDC injection (PDC ipsi) while being unaffected in the contralateral one (PDC contra) at all time points examined. Data are expressed as percentage of sham at each corresponding dpi. Sham, n = 5; PDC, $n = 8$; two-way repeated measures ANOVA analysis (Glu: $F_{group}(2,18) = 66.92$, $P < 0.0001$; Gln: $F_{group}(2,18) = 47.69$, $P < 0.0001$) followed by Tukey's multiple comparisons post-test (*$P < 0.05$, ****$P < 0.0001$ vs. sham; $^{\$\$\$}P < 0.001$, $^{\$\$\$\$}P < 0.0001$ ipsi vs. contra). Boxes represent the 25th and 75th percentile (bar = median), whiskers show the min and max values. (For interpretation of the references to colour in this figure legend, the reader is referred to the web version of this article.)

3.3. Impact of unilateral intranigral PDC injection at STN level

3.3.1. Glutamate and glutamine levels

^{1}H-MRSI spectra were analyzed in voxels centered on the right and the left STN of sham and PDC animals (Fig. 5A). Metabolic changes were followed at 30, 60 and 120 dpi. Levels of Glu (Fig. 5B, left graph) and of Gln (Fig. 5B, right graph) in the STN ipsilateral to PDC did not differ significantly from sham values at 30 and 60 dpi but were enhanced at 120 dpi. In the contralateral STN, Gln levels were increased vs. sham at 60 and 120 dpi and were significantly higher at these time points than the levels measured in the ipsilateral STN (Fig. 5B**, right graph**).

3.3.2. Intraneuronal COI mRNA levels

Quantitative in situ hybridization analysis of intraneuronal COI mRNA levels in the STN is presented in Fig. 5C. COI mRNA levels were not significantly modified in the STN ipsilateral to PDC injection at 4 and 30 dpi but were increased by 32.5% at 120 dpi vs. values from sham animals. In the contralateral STN, intraneuronal COI mRNA levels were significantly increased vs. control at 4 (+34%), 30 (+26%) and 120 dpi (+74%). When compared to the ipsilateral STN, contralateral STN showed higher COI mRNA levels at all the time points examined but the difference was significant only at 30 dpi. Fig. 5D provides an illustration of the bilateral increase in intraneuronal levels of COI mRNA at 120 dpi.

3.4. Impact of contralateral STN lesion on the motor dysfunction, the loss of dopamine neurons and the striatal metabolite levels in the unilateral PDC-induced model of parkinsonism

The extensive STN lesion produced by ibotenic acid injection in the selected PDC + ibot animals is illustrated in Fig. 6A.

3.4.1. Behavioral analysis

PDC + ibot animals showed an asymmetry score close to zero at 120 dpi, which did not differ from sham and was markedly reduced versus PDC animals (Fig. 6B). These results indicate that lesion of the STN contralateral to the primary injured site prevents the onset of akinesia-like deficits in the PDC model of progressive asymmetrical parkinsonism.

3.4.2. Loss of nigral TH neurons at 120 dpi

In the sham animals, the estimated mean number of TH-positive neurons in the SNc region analyzed was of 4325.1 ± 152.4. Compared to sham, the PDC + ibot animals showed a modest decrease in the number of nigral TH-positive neurons of around 20% in both brain sides at 120 dpi, consistent with the lack of asymmetry in the cylinder test (Fig. 6C). The loss of TH neurons in these animals was markedly lower than the one measured in the PDC animals for the PDC-injected SNc (20% vs. 50%), as illustrated in Fig. 6D, while it was equivalent for the uninjected SNc (Fig. 6C). These data thus suggest that contralateral STN lesion halts the loss of dopamine neurons in the primary injured SNc but does not prevent the initiation of the degenerative process in the uninjected SNc.

3.4.3. Striatal glutamate and glutamine concentrations measured by ^{1}H-MRSI at 120 dpi and relationship with TH neuron loss

In the striatum ipsilateral to PDC injection, the levels of Glu were significantly lower in the PDC + ibot vs. PDC animals and did not differ from sham. The levels of Gln were also normalized, but the decrease vs. PDC did not reach significance (Fig. 6E). Interestingly, correlative analysis including the PDC, PDC + ibot and the sham groups shows a strong negative correlation between the concentrations of these metabolites in the striatum and the numbers of TH-positive neurons in the SNc (Fig. 6F).

4. Discussion

The corticostriatal pathway, which provides the striatum with a heavy glutamatergic innervation, and the STN, the only intrinsic glutamatergic component of the basal ganglia, are considered as key players in the development of PD motor symptoms and in the progression of the disease. To date, most published studies relate to abnormalities in the activity of these glutamatergic systems in the side ipsilateral to the lesion in models of acute and extensive unilateral dopaminergic degeneration, such as induced by intranigral 6-hydroxydopamine, when the pathological state was stabilized at a maximal level. There is also evidence for functional alterations of either or both of these components before symptom onset under such extensive lesion condition and in partial lesion models, either unilateral or bilateral, showing moderate motor abnormalities, suggesting that they might be early phenomena in PD pathophysiology (Breysse et al., 2003; Paille et al., 2010; Schirinzi et al., 2016). However, PD has a progressive course, characterized by an asymmetrical bilateral evolution of the dopaminergic degeneration and unilateral onset of motor symptoms, contralateral to the most damaged brain hemisphere. Such complex natural history raises the question of the reactivity of these glutamatergic systems on both brain sides from presymptomatic to symptomatic state in an asymmetrically evolving neurodegeneration context. Here, we addressed this issue in the progressive model based on pharmacologically induced dysfunction of EAATs by unilateral intranigral PDC injection. We previously reported that this model is characterized by a uni- to bilateral evolution of the neurodegeneration and an onset of akinesia-like deficit of the contralateral forepaw when the loss of dopaminergic neurons reaches 50–60% in the injected SN and also affects to a less extent the uninjected side (20–30%) (Assous et al., 2014). The present results regarding the striatum and the STN of the side ipsilateral to the intranigral PDC injection, i.e. contralateral to motor deficit onset, are more or less consistent with the literature data. The most unexpected findings concern the STN contralateral to PDC injection, which shows an early and sustained reactivity and whose lesion slows down dopamine neuron loss in the primary injured SN. These data support the view that maladaptive interhemispheric mechanisms involving the STN may contribute to the evolution of the neurodegenerative process.

The corticostriatal pathway represents the main excitatory input to the striatum, providing information from diverse cortical areas whose processing through the basal ganglia network plays a major role in motor control but also in cognitive function. This input is bilateral, with an ipsilateral dominance, and topographically organized. The two classical forms of long-term plasticity, LTP and LTD, as well as short-term forms of plasticity are expressed at corticostriatal synapses and are considered as substrates of motor learning and behavior (Di Filippo et al., 2009). Abnormalities of corticostriatal synaptic transmission and plasticity have long been associated with basal ganglia-related movement disorders, including PD, Huntington's disease and L-DOPA-induced dyskinesia (Calabresi et al., 2000a; Calabresi et al., 2000b; Iravani et al., 2012). In animal models of PD, differential alterations have been reported among toxin-induced models, depending on the dopaminergic lesion extent, as well as among genetic models. Acute extensive toxin-induced lesion of the nigrostriatal pathway, which triggers robust motor deficits, results in increased corticostriatal glutamatergic transmission and in the loss of both LTP and LTD, while partial lesion, triggering mild deficit, results in the specific loss of LTP (Paille et al., 2010). In genetic models exhibiting subtle motor abnormalities and quite no degeneration, either both forms of plasticity or LTD are altered (Madeo et al., 2012). In the current study, we examined corticostriatal transmission and plasticity in the PDC-injected hemisphere at 120 dpi, a time point at which significant contralateral motor deficit is measured in the cylinder test, associated with partial bilateral loss of dopamine neurons, predominant in the injected SN. The results show increased corticostriatal transmission and loss of both LTP and LTD, as previously reported in rat 6-

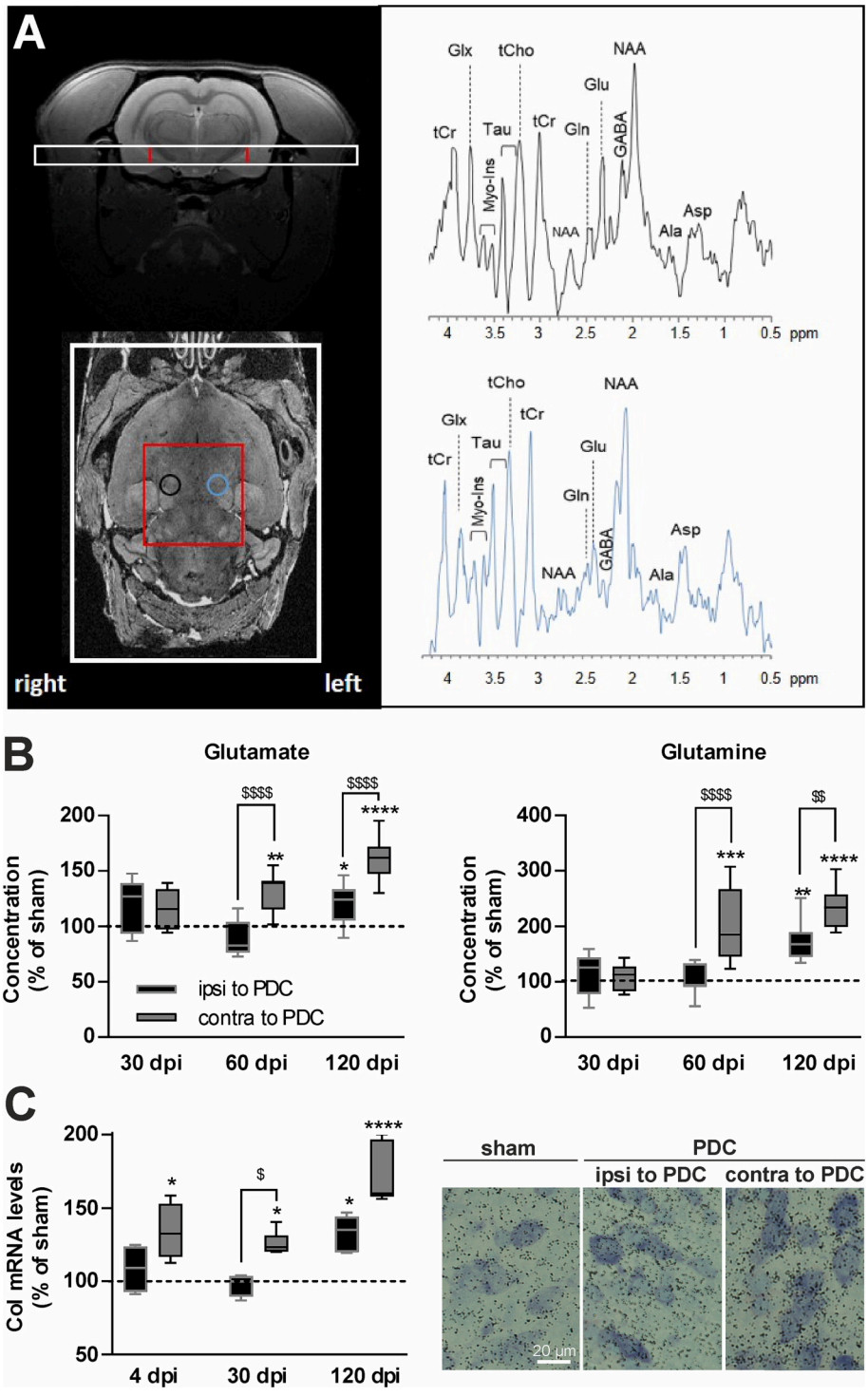

(caption on next page)

Fig. 5. Metabolic changes in the STN of unilateral PDC animals.
(A) In vivo ^{1}H-MRSI in the STN. On the morphological coronal (at the top) and axial (at the bottom) T2-weighted MR images is shown the position of the 2D MRSI grid (red labelling) with the regions of interest covering the STN of both brain sides. Representative ^{1}H-MRSI spectra obtained on a PDC rat in the STN of the right hemisphere (black voxel) and the left hemisphere (blue voxel), which correspond to the sides contralateral and ipsilateral to PDC injection, respectively, are displayed on the left. For abbreviations, see Fig. 4.
(B) STN levels of Glu (left graph) and Gln (right graph) measured by in vivo ^{1}H-MRSI at 30, 60 and 120 dpi. In the STN ipsilateral to intranigral PDC injection (PDC ipsi), the only significant change vs. corresponding sham is an increase in Gln concentration at 120 dpi. In the STN contralateral to PDC, concentrations of both Glu and Gln are increased vs. sham values from 60 dpi. Data are expressed as percentage of sham at each corresponding dpi. Sham, n = 5; PDC, n = 8; two-way repeated measures ANOVA analysis (Glu: $F_{group}(2,18) = 29.73$, $P < 0.0001$; $F_{dpi}(2,36) = 6.472$, $P = 0.004$; $F_{interaction}(4,36) = 6.784$, $P = 0.0004$; Gln: $F_{group}(2,18) = 22.53$, $P < 0.0001$; $F_{dpi}(2,36) = 14.11$, $P < 0.0001$; $F_{interaction}(4,36) = 6.932$, $P = 0.0003$) followed by Tukey's multiple comparisons post-test (*$P < 0.05$, **$P < 0.01$; ***$P < 0.001$, ****$P < 0.0001$ vs. sham, $^{\$\$}P < 0.01$, $^{\$\$\$\$}P < 0.0001$ ipsi vs. contra to PDC).
(C) Intraneuronal COI mRNA levels in the STN. On the left, quantitative in situ hybridization analysis at 4, 30 and 120 dpi. COI mRNA levels show significant increase vs. sham from 4 dpi in the STN contralateral to PDC injection but only at 120 dpi in the ipsilateral STN. Sham, n = 7; PDC 4 dpi, n = 4, 30 dpi, $n = 6$, 120 dpi, n = 5; Kruskal-Wallis ANOVA analysis ($P < 0.0001$) followed by Dunn's multiple comparisons post-test (*$P < 0.05$, ****$P < 0.0001$ vs. sham, $^{\$}P < 0.05$ PDC ipsi vs. contra). Boxes in **B** and **C** represent the 25th and 75th percentile (bar = median), whiskers show the min and max values.
On the right, bright-field photomicrograph at high magnification of toluidine blue-counterstained sections illustrating COI mRNA intraneuronal labeling in the STN of a PDC animal at 120 dpi compared to sham. Note the higher number of silver grains per labeled neurons in the STN of both brain sides vs. sham. (For interpretation of the references to colour in this figure legend, the reader is referred to the web version of this article.)

hydroxydopamine PD models with complete dopaminergic degeneration (Bagetta et al., 2010; Centonze et al., 2001; Chassain et al., 2016; Gubellini et al., 2002; Tang et al., 2001). In the present study, we did not differentiate the two subpopulations of SPNs that are distinguished based on their preferential expression of D1 or D2 dopamine receptors, which modulate corticostriatal glutamatergic plasticity in complex and opposite ways (for review, see (Calabresi et al., 2007)). An abundant literature suggests that SPNs uniformly express LTP and LTD induced by different protocols both in the rat (Calabresi et al., 1992a; Calabresi et al., 1992b; Charpier and Deniau, 1997; Chassain et al., 2016; Fino et al., 2005; Lovinger, 2010; Lovinger et al., 1993; Pawlak and Kerr, 2008) and in mouse (Bagetta et al., 2011; Shen et al., 2008). To our knowledge, whether these two forms of synaptic plasticity are differentially affected in 6-hydroxydopamine-lesioned rats in D1 vs. D2 SPNs has not been determined, while a study in transgenic mouse shows that LTP is selectively lost in D1 and LTD in D2 SPNs (Thiele et al., 2014).

We also performed longitudinal in vivo metabolic imaging using ^{1}H-MRSI at 30, 60 and 120 dpi. This technique offers a noninvasive means for simultaneous quantification in vivo of several metabolites in specific brain areas, with several applications for studying brain metabolism and pathological dysfunctions both in human and animal models (Ajram et al., 2019; Hangel et al., 2022; Maudsley et al., 2021; Rae, 2014). For example, ^{1}H-MRSI has been used to assess metabolic changes in the striatum and/or the SN of parkinsonian patients (Groger et al., 2014) and in animal PD models (Klietz et al., 2019). High magnetic field (11.7 T) and MAPSHIM procedure to homogenize the magnetic field at the area of interest, as utilized here, can improve both the spectral separation and the signal to noise ratio, which results in higher and narrower spectral peaks in an acquisition time compatible with in vivo experiments in animals. Hence, signals that are difficult to quantify at lower field strengths can be estimated more easily. In particular, Glu and Gln can be quantified separately instead of their sum termed Glx (Hangel et al., 2022). Because ^{1}H-MRSI does not allow discriminating between intracellular and extracellular Glu nor between metabolic and neurotransmitter pools, measures cannot be directly attributed to a specific function. However, there is evidence suggesting that MRS-visible Glu reflects metabolic activity linked to glutamatergic neurotransmission (Rae, 2014; Stagg et al., 2011; Yuksel and Ongur, 2010). Our results showed that glutamate and glutamine levels are markedly increased in the striatum ipsilateral to the PDC injection at all time points, while being unaffected in the contralateral striatum. These results confirm and extend previous data obtained in the unilateral 6-hydroxydopamine and the bilateral MPTP models (Chassain et al., 2010; Chassain et al., 2016; Melon et al., 2015), by suggesting that changes in glutamate metabolism might occur in the striatum of the primary injured side from presymptomatic stage with moderate dopamine neuron loss. The lack of change in the contralateral striatum suggests that the 20% neuronal loss in the uninjected SN is below the threshold for the alteration of striatal glutamate metabolism. Whether, in such condition, corticostriatal transmission and plasticity are nevertheless altered in the contralateral hemisphere is an intriguing issue that remains to be addressed.

Changes in firing rate, pattern, and oscillation of STN neurons have been observed in PD patients and dopamine-depleted animal models (see (Quiroga-Varela et al., 2013)). Despite discrepancies in the parameters affected among studies, attributable to factors such as the PD stage (Remple et al., 2011), the level of dopamine depletion or the lesion model, abnormal activity of STN is considered as a key substrate of PD symptoms. Consistently, the surgical treatment of PD by deep brain stimulation targeting the STN provides highly effective relief of motor symptoms (Benabid et al., 2009; Limousin et al., 1995); it is also suspected to have neuroprotective disease-modifying potential (Guridi et al., 2018; Harnack and Kupsch, 2010; McKinnon et al., 2019; Torres et al., 2017). Changes in the functioning of STN neurons have been also detected by measurements of the activity or mRNA levels of COI, a metabolic marker of neuronal activity. Interestingly, increased levels of COI mRNA have been consistently reported to occur in primate and rodent PD models, both under extensive and partial neurodegeneration conditions when the lesion was stabilized (Breysse et al., 2003; Hirsch et al., 2000; Vila et al., 1997; Vila et al., 2000). A time-course study also showed enhanced COI mRNA expression at early stage in the course of the degeneration, preceding changes in firing activity (Vila et al., 2000). We thus used this index to perform a time course study of STN function in the PDC model at 4, 30 and 120 dpi. In the STN ipsilateral to the injection, significant increase in COI mRNA levels occurred only at the symptomatic stage of 120 dpi. These data do not fit with results obtained in the 6-hydroxydopamine model, showing increased levels from 24 h post-injection (Vila et al., 2000), which could be due to the slower kinetics of the degenerative process in the PDC model. However, they are in line with the implication of abnormal STN activity in the appearance of motor deficits. Surprisingly, in the STN contralateral to PDC injection, we found an early and sustained increase in COI mRNA levels as soon as at 4 dpi, thus far before any loss of dopamine neurons in the uninjected SN. This increase is maintained overtime and is even stronger than that of the STN ipsilateral to PDC injection. The present longitudinal study of Glu and Gln levels by ^{1}H-MRSI provides additional evidence for earlier and stronger metabolic changes in the contralateral STN. Indeed, while only Gln is increased in the ipsilateral STN at 120 dpi, both Glu and Gln levels are enhanced in the contralateral STN from 60 dpi. Contrary to the reactivity of the ipsilateral STN, the reactivity of the contralateral STN obviously does not translate into motor impairment, as the akinesia-like deficit affects the forepaw contralateral to the primary injured SN. It could be that the functional output of the changes in STN activity depends on a threshold in the damage of the dopamine system on the same brain side; in other words, contralateral STN overactivity might be

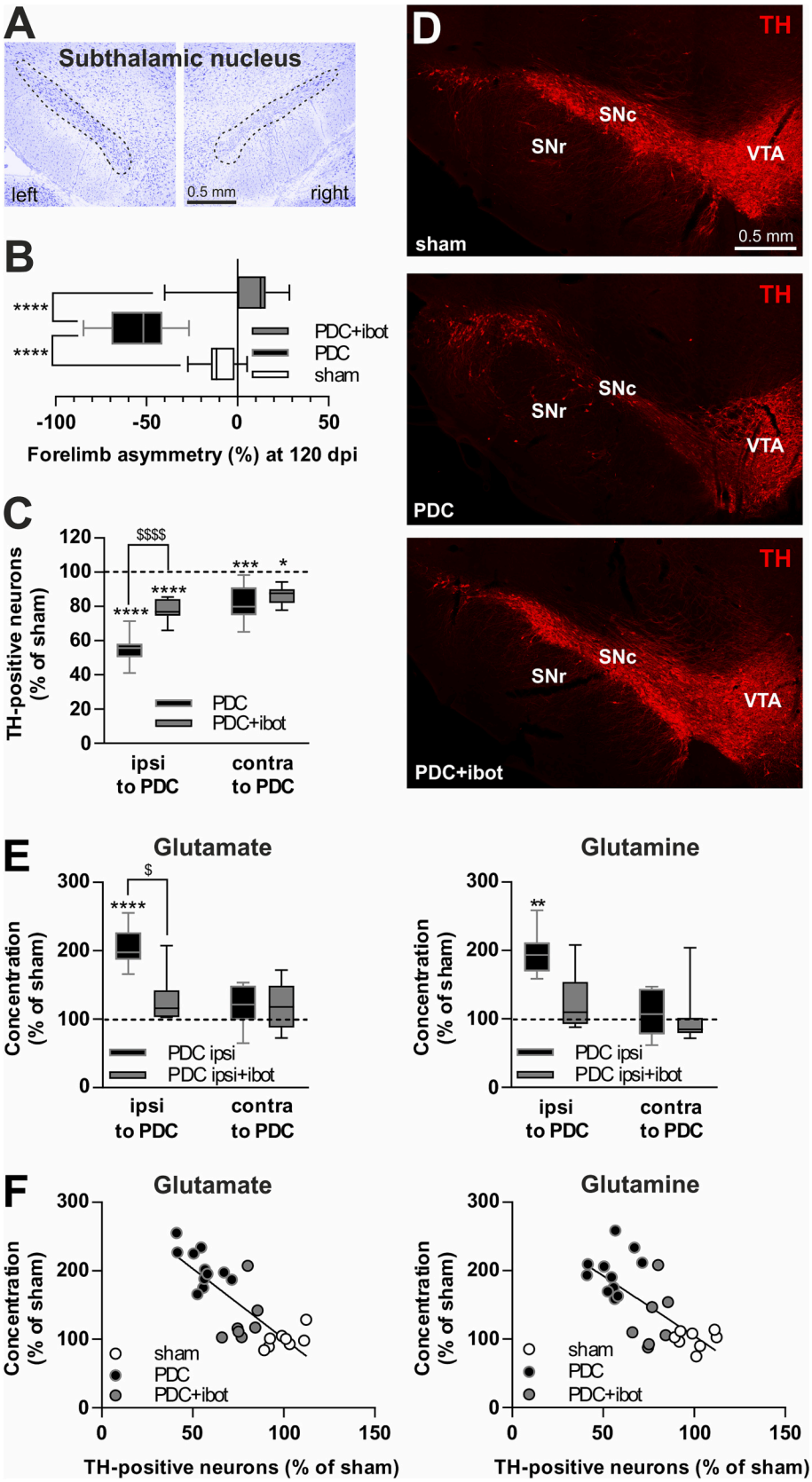

(caption on next page)

Fig. 6. Impact of contralateral STN lesion on the PDC-induced behavioral deficit, nigral dopamine neuron loss and striatal increases of glutamate and glutamine levels.

(A) Photomicrographs of a Nissl-stained section illustrating the extent of the ibotenic acid-induced lesion of the STN (delineated by dotted lines) in a selected PDC + ibot animal. Note the massive cell loss in the in the injected (right image) versus uninjected (left image) STN.

(B) Forelimb asymmetry in animals with unilateral PDC injection alone (PDC) followed by ibotenate-induced lesion of the contralateral STN (PDC + ibot). Asymmetry scores were determined at 120 days post PDC injection. A significant bias towards the use of the ipsilateral forepaw, reflecting akinesia of the contralateral forepaw, is measured in PDC rats vs. sham. This bias is no more observed in the PDC + ibot animals, their asymmetry score, close to 0, being not significantly different from sham values and significantly different from PDC animals. Sham, n = 8; PDC, *n* = 11; PDC + ibot, n = 7; one-way ANOVA analysis ($F(2,23) = 29.69$, $P < 0.0001$) followed byTukey's multiple comparisons test (****$P < 0.0001$).

(C) Loss of TH neurons in the substantia nigra of both brain sides (ipsi and contra to PDC) induced by unilateral PDC injection alone (PDC) or followed by contralateral STN lesion (PDC + ibot). Cell counts were performed at 120 days post PDC injection. PDC + ibot animals show significantly lower cell loss in the primary injured substantia nigra (ipsi to PDC) and equivalent cell loss in the contralateral nigra compared to those of the PDC group. Sham, n = 8; PDC, n = 11; PDC + ibot, n = 7; one-way ANOVA analysis ($F(4,39) = 36.66$ $P < 0.0001$) followed by Sidak's multiple comparisons post-test (*$P < 0.05$, ***$P < 0.001$, ****$P < 0.0001$ vs. sham, $^{\$\$\$\$}P < 0.0001$ PDC vs. PDC + ibot).

(D) Photomicrographs of TH-immunostained sections of sham, PDC and PDC + ibot animals at the level of the injected nigra. Note the lower loss of dopaminergic neurons in the PDC + ibot condition compared to PDC alone. SNc: substantia nigra *pars compacta*; SNr: substantia nigra *pars reticulata*; VTA: ventral tegmental area.

(E) Striatal levels of glutamate (left graph) and glutamine (right graph) measured at 120 dpi by ^{1}H-MRSI in PDC and PDC + ibot rats. Note that contralateral STN lesion normalizes the level of these metabolites in the striatum ipsilateral to intranigral PDC injection. Kruskal-Wallis ANOVA analysis ($P < 0.0001$) followed by Dunn's multiple comparisons post-test (**$P < 0.01$, ****$P < 0.0001$ vs. sham, $^{\$}P < 0.05$ PDC vs. PDC + ibot).

(F) Relationships between glutamate (left graph) and glutamine (right graph) concentration and TH-positive cell number. Spearman test shows a highly significant negative correlation (Glu: $r = -0.777$, $P < 0.0001$; Gln: $r = -0.671$, $P = 0.0002$), meaning that the metabolites' concentration increases as the number of TH-positive cells decreases. In **E** and **F**: sham, n = 8; PDC, n = 11; PDC + ibot, *n* = 7.

Boxes in **B**, **C** and **E** represent the 25th and 75th percentile (bar = median), whiskers show the min and max values.

balanced by the maintenance of a sufficient dopamine tone on the basal ganglia network of the same hemisphere.

An important question is whether the sustained reactivity of the contralateral STN plays a role in the evolution of the neurodegenerative process. It has been previously hypothesized that enhanced glutamatergic input to contralateral SNc neurons might initiate the contralateral degeneration in the PD model based on unilateral injection of α-synuclein preformed fibrils in the striatum (Patterson et al., 2019). If this was the case in our model, contralateral STN lesion should prevent the uni- to bilateral evolution of the PDC-induced neurodegeneration. We performed this lesion at an early stage of the degenerative process triggered by unilateral intranigral PDC injection, i.e., at 7 dpi, and examined the impact on nigral DA neuron loss at 120 dpi. This timing was determined from our previous work showing that significant neuronal death occurs as soon as 4 dpi in the injected SN, while it is markedly delayed in the contralateral SN (significant effect at 60 dpi) (Assous et al., 2014). Unexpectedly, contralateral STN lesion did not prevent cell death initiation in the SN of the same hemisphere, but halted the ongoing degeneration in the PDC-injected SN and prevented the appearance of the motor deficit. For instance, whereas at 120 dpi the PDC animals showed predominant neuronal loss in the injected SN, reaching >50% of the total population, the PDC + ibot animals showed equivalent modest cell loss on both brain sides, and no more motor asymmetry in the cylinder test. Moreover, STN lesion also normalized the striatal levels of Glu and Gln. These findings point to hyperactivity of the contralateral STN as a main mechanism sustaining the progression of dopamine neurodegeneration initiated by intranigral PDC and subsequent behavioral and metabolic changes. Identifying the anatomical pathways and molecular mechanisms underlying this hyperactivity and the subsequent neuronal death it triggers, and determining whether such adaptive interhemispheric mechanism may also play a role in other progressive models of PD, remain critical issues to be addressed in the future to better understand the pathophysiology of PD. Although ipsilateral STN connections are prominent, there is evidence for bilateral and interhemispheric STN connections (Castle et al., 2005; Cavdar et al., 2018), including afferent inputs from thalamic and brainstem structures, which may provide routes for the implication of this structure in interhemispheric adaptive changes. In this line, the fact that unilateral STN surgery affects contralateral STN activity and has bilateral motor effects supports the view that one side of the basal ganglia can influence the functioning of the other (Brun et al., 2012).

In conclusion, this study reveals complex pathological cross-talks between the STN and SN of both hemispheres, whose substrates remain to be identified, that could be involved both in the cell death evolution and the appearance of PD symptoms. Therefore, targeting these interhemispheric mechanisms might have disease-modifying effects, opening novel therapeutic perspectives.

Authors' roles

PS, CC, CM, PG, FD and LKLG contributed to the study conception and experimental design, with FD and LKLG supervising the work. CM and PS carried out the stereotaxic surgeries and immunohistochemical experiments. PS performed the in situ hybridization study and analysis. CM and CC conducted the behavioral study and data analyses. PG performed the electrophysiological recordings and analysis. CC performed the longitudinal ^{1}H-MRSI study and contributed with BP, YLF and GP to data analysis. All authors contributed to the result presentation and interpretation. LKLG wrote the manuscript with the help of PS, CC, CM, PG, and FD for review and editing. All authors reviewed and agreed the final version of the paper.

Funding

This work was funded by a grant from France Parkinson (to LKLG) and from St. Jude Medical™ (to FD), and was supported by the CNRS, Aix-Marseille University and Clermont Auvergne University.

CRediT authorship contribution statement

Pascal Salin: Conceptualization, Data curation, Investigation, Methodology, Writing – review & editing, Writing – original draft. **Christophe Melon:** Data curation, Investigation, Methodology, Writing – review & editing. **Carine Chassain:** Conceptualization, Data curation, Investigation, Methodology, Writing – original draft, Writing – review & editing. **Paolo Gubellini:** Conceptualization, Data curation, Investigation, Methodology, Writing – original draft, Writing – review & editing. **Guilhem Pages:** Data curation, Investigation, Methodology, Writing – review & editing. **Bruno Pereira:** Data curation, Methodology, Writing – review & editing. **Yann Le Fur:** Data curation, Methodology, Writing – review & editing. **Franck Durif:** Conceptualization, Funding acquisition, Supervision, Writing – original draft, Writing – review & editing. **Lydia Kerkerian-Le Goff:** Conceptualization, Data curation, Funding acquisition, Methodology, Project administration, Supervision, Validation, Writing – original draft, Writing – review & editing.

Declaration of competing interest

None.

Data availability

Data will be made available on request.

Acknowledgments

Microscopy was performed at the imaging platform of the IBDM and we acknowledge France-BioImaging Infrastructure (ANR-10-INSB-04-01). This work has received support from the French government under the "France 2030" program via A*Midex (Initiative d'Excellence d'Aix-Marseille Université, AMX-19-IET-004) and ANR funding (ANR-17-EURE-0029). It was a part of the research program of the Centre of Excellence DHUNE, which was supported by the French National Plan on Neurodegenerative Diseases funded by the French Ministry of Higher Education and Research and the «Investissements d'Avenir» program.

References

Ajram, L.A., Pereira, A.C., Durieux, A.M.S., Velthius, H.E., Petrinovic, M.M., McAlonan, G.M., 2019. The contribution of [1H] magnetic resonance spectroscopy to the study of excitation-inhibition in autism. Prog. Neuro-Psychopharmacol. Biol. Psychiatry 89, 236–244.

Aoyama, K., Matsumura, N., Watabe, M., Nakaki, T., 2008. Oxidative stress on EAAC1 is involved in MPTP-induced glutathione depletion and motor dysfunction. Eur. J. Neurosci. 27, 20–30.

Assous, M., Had-Aissouni, L., Gubellini, P., Melon, C., Nafia, I., Salin, P., Kerkerian-Le-Goff, L., Kachidian, P., 2014. Progressive parkinsonism by acute dysfunction of excitatory amino acid transporters in the rat substantia nigra. Neurobiol. Dis. 65, 69–81.

Bacci, J.J., Kerkerian-Le Goff, L., Salin, P., 2002. Effects of intralaminar thalamic nuclei lesion on glutamic acid decarboxylase (GAD65 and GAD67) and cytochrome oxidase subunit I mRNA expression in the basal ganglia of the rat. Eur. J. Neurosci. 15, 1918–1928.

Bagetta, V., Ghiglieri, V., Sgobio, C., Calabresi, P., Picconi, B., 2010. Synaptic dysfunction in Parkinson's disease. Biochem. Soc. Trans. 38, 493–497.

Bagetta, V., Picconi, B., Marinucci, S., Sgobio, C., Pendolino, V., Ghiglieri, V., Fusco, F.R., Giampa, C., Calabresi, P., 2011. Dopamine-dependent long-term depression is expressed in striatal spiny neurons of both direct and indirect pathways: implications for Parkinson's disease. J. Neurosci. 31, 12513–12522.

Barrett, M.J., Wylie, S.A., Harrison, M.B., Wooten, G.F., 2011. Handedness and motor symptom asymmetry in Parkinson's disease. J. Neurol. Neurosurg. Psychiatry 82, 1122–1124.

Benabid, A.L., Chabardes, S., Mitrofanis, J., Pollak, P., 2009. Deep brain stimulation of the subthalamic nucleus for the treatment of Parkinson's disease. Lancet Neurol. 8, 67–81.

Berman, A.E., Chan, W.Y., Brennan, A.M., Reyes, R.C., Adler, B.L., Suh, S.W., Kauppinen, T.M., Edling, Y., Swanson, R.A., 2011. N-acetylcysteine prevents loss of dopaminergic neurons in the EAAC1−/− mouse. Ann. Neurol. 69, 509–520.

Blandini, F., Porter, R.H., Greenamyre, J.T., 1996. Glutamate and Parkinson's disease. Mol. Neurobiol. 12, 73–94.

Blesa, J., Przedborski, S., 2014. Parkinson's disease: animal models and dopaminergic cell vulnerability. Front. Neuroanat. 8, 155.

Bohnen, N.I., Albin, R.L., Koeppe, R.A., Wernette, K.A., Kilbourn, M.R., Minoshima, S., Frey, K.A., 2006. Positron emission tomography of monoaminergic vesicular binding in aging and Parkinson disease. J. Cereb. Blood Flow Metab. 26, 1198–1212.

Borghammer, P., 2021. The alpha-Synuclein origin and connectome model (SOC model) of Parkinson's disease: explaining motor asymmetry, non-motor phenotypes, and cognitive decline. J. Parkinsons Dis. 11, 455–474.

Breysse, N., Amalric, M., Salin, P., 2003. Metabotropic glutamate 5 receptor blockade alleviates akinesia by normalizing activity of selective basal-ganglia structures in parkinsonian rats. J. Neurosci. 23, 8302–8309.

Brun, Y., Karachi, C., Fernandez-Vidal, S., Jodoin, N., Grabli, D., Bardinet, E., Mallet, L., Agid, Y., Yelnik, J., Welter, M.L., 2012. Does unilateral basal ganglia activity functionally influence the contralateral side? What we can learn from STN stimulation in patients with Parkinson's disease. J. Neurophysiol. 108, 1575–1583.

Calabresi, P., Maj, R., Pisani, A., Mercuri, N.B., Bernardi, G., 1992a. Long-term synaptic depression in the striatum: physiological and pharmacological characterization. J. Neurosci. 12, 4224–4233.

Calabresi, P., Pisani, A., Mercuri, N.B., Bernardi, G., 1992b. Long-term potentiation in the striatum is unmasked by removing the voltage-dependent magnesium block of Nmda receptor channels. Eur. J. Neurosci. 4, 929–935.

Calabresi, P., Mercuri, N.B., Sancesario, G., Bernardi, G., 1993. Electrophysiology of dopamine-denervated striatal neurons. Implications for Parkinson's disease. Brain 116 (Pt 2), 433–452.

Calabresi, P., Centonze, D., Gubellini, P., Marfia, G.A., Pisani, A., Sancesario, G., Bernardi, G., 2000a. Synaptic transmission in the striatum: from plasticity to neurodegeneration. Prog. Neurobiol. 61, 231–265.

Calabresi, P., Giacomini, P., Centonze, D., Bernardi, G., 2000b. Levodopa-induced dyskinesia: a pathological form of striatal synaptic plasticity? Ann. Neurol. 47, S60–S68 (discussion S68-69).

Calabresi, P., Picconi, B., Tozzi, A., Di Filippo, M., 2007. Dopamine-mediated regulation of corticostriatal synaptic plasticity. Trends Neurosci. 30, 211–219.

Castle, M., Aymerich, M.S., Sanchez-Escobar, C., Gonzalo, N., Obeso, J.A., Lanciego, J.L., 2005. Thalamic innervation of the direct and indirect basal ganglia pathways in the rat: Ipsi- and contralateral projections. J. Comp. Neurol. 483, 143–153.

Cavdar, S., Ozgur, M., Cakmak, Y.O., Kuvvet, Y., Kunt, S.K., Saglam, G., 2018. Afferent projections of the subthalamic nucleus in the rat: emphasis on bilateral and interhemispheric connections. Acta Neurobiol. Exp. (Wars) 78, 251–263.

Centonze, D., Picconi, B., Gubellini, P., Bernardi, G., Calabresi, P., 2001. Dopaminergic control of synaptic plasticity in the dorsal striatum. Eur. J. Neurosci. 13, 1071–1077.

Charpier, S., Deniau, J.M., 1997. In vivo activity-dependent plasticity at cortico-striatal connections: evidence for physiological long-term potentiation. Proc. Natl. Acad. Sci. U. S. A. 94, 7036–7040.

Chassain, C., Bielicki, G., Keller, C., Renou, J.P., Durif, F., 2010. Metabolic changes detected in vivo by 1H MRS in the MPTP-intoxicated mouse. NMR Biomed. 23, 547–553.

Chassain, C., Melon, C., Salin, P., Vitale, F., Couraud, S., Durif, F., Kerkerian-Le Goff, L., Gubellini, P., 2016. Metabolic, synaptic and behavioral impact of 5-week chronic deep brain stimulation in hemiparkinsonian rats. J. Neurochem. 136, 1004–1016.

Cheung, Z.H., Ip, N.Y., 2009. The emerging role of autophagy in Parkinson's disease. Mol. Brain 2, 29.

Choe, B.Y., Park, J.W., Lee, K.S., Son, B.C., Kim, M.C., Kim, B.S., Suh, T.S., Lee, H.K., Shinn, K.S., 1998. Neuronal laterality in Parkinson's disease with unilateral symptom by in vivo 1H magnetic resonance spectroscopy. Investig. Radiol. 33, 450–455.

Claassen, D.O., McDonell, K.E., Donahue, M., Rawal, S., Wylie, S.A., Neimat, J.S., Kang, H., Hedera, P., Zald, D., Landman, B., Dawant, B., Rane, S., 2016. Cortical asymmetry in Parkinson's disease: early susceptibility of the left hemisphere. Brain Behav. 6, e00573.

Dauer, W., Przedborski, S., 2003. Parkinson's disease: mechanisms and models. Neuron 39, 889–909.

De Groot, J., 1959. The Rat Forebrain in Stereotaxic Coordinates. AFD Natuurkunde N. V. Noord-Hallandsche Wetgevers Maatschappij. Verhandelingen der Koninklijke Nederlandse Akademic van Wetenschappen, Amsterdam.

Di Filippo, M., Picconi, B., Tantucci, M., Ghiglieri, V., Bagetta, V., Sgobio, C., Tozzi, A., Parnetti, L., Calabresi, P., 2009. Short-term and long-term plasticity at corticostriatal synapses: implications for learning and memory. Behav. Brain Res. 199, 108–118.

Dinh, E., Rival, T., Carrier, A., Asfogo, N., Corti, O., Melon, C., Salin, P., Lortet, S., Kerkerian-Le Goff, L., 2021. TP53INP1 exerts neuroprotection under ageing and Parkinson's disease-related stress condition. Cell Death Dis. 12, 460.

Djaldetti, R., Ziv, I., Melamed, E., 2006. The mystery of motor asymmetry in Parkinson's disease. Lancet Neurol. 5, 796–802.

Fedorova, T.D., Knudsen, K., Horsager, J., Hansen, A.K., Okkels, N., Gottrup, H., Vang, K., Borghammer, P., 2023. Dopaminergic dysfunction is more symmetric in dementia with Lewy bodies compared to Parkinson's disease. J. Parkinsons Dis. 13, 515–523.

Finlay, C., Duty, S., 2014. Therapeutic potential of targeting glutamate receptors in Parkinson's disease. J. Neural Transm. (Vienna) 121, 861–880.

Fino, E., Glowinski, J., Venance, L., 2005. Bidirectional activity-dependent plasticity at corticostriatal synapses. J. Neurosci. 25, 11279–11287.

Foffani, G., Obeso, J.A., 2018. A cortical pathogenic theory of Parkinson's disease. Neuron 99, 1116–1128.

Garrido, A., Iranzo, A., Stefani, A., Serradell, M., Munoz-Lopetegi, A., Marrero, P., Hogl, B., Gaig, C., Santamaria, J., Tolosa, E., Poewe, W., Sleep Innsbruck Barcelona, G., 2020. Lack of asymmetry of nigrostriatal dopaminergic function in healthy subjects. Mov. Disord. 35, 1072–1076.

Groger, A., Kolb, R., Schafer, R., Klose, U., 2014. Dopamine reduction in the substantia nigra of Parkinson's disease patients confirmed by in vivo magnetic resonance spectroscopic imaging. PLoS One 9, e84081.

Gubellini, P., Kachidian, P., 2015. Animal models of Parkinson's disease: an updated overview. Rev. Neurol. (Paris) 171, 750–761.

Gubellini, P., Picconi, B., Bari, M., Battista, N., Calabresi, P., Centonze, D., Bernardi, G., Finazzi-Agro, A., Maccarrone, M., 2002. Experimental parkinsonism alters endocannabinoid degradation: implications for striatal glutamatergic transmission. J. Neurosci. 22, 6900–6907.

Gubellini, P., Eusebio, A., Oueslati, A., Melon, C., Kerkerian-Le Goff, L., Salin, P., 2006. Chronic high-frequency stimulation of the subthalamic nucleus and L-DOPA treatment in experimental parkinsonism: effects on motor behaviour and striatal glutamate transmission. Eur. J. Neurosci. 24, 1802–1814.

Guridi, J., Rodriguez-Rojas, R., Carmona-Abellan, M., Parras, O., Becerra, V., Lanciego, J. L., 2018. History and future challenges of the subthalamic nucleus as surgical target: review article. Mov. Disord. 33, 1540–1550.

Had-Aissouni, L., 2012. Toward a new role for plasma membrane sodium-dependent glutamate transporters of astrocytes: maintenance of antioxidant defenses beyond extracellular glutamate clearance. Amino Acids 42, 181–197.

Hangel, G., Niess, E., Lazen, P., Bednarik, P., Bogner, W., Strasser, B., 2022. Emerging methods and applications of ultra-high field MR spectroscopic imaging in the human brain. Anal. Biochem. 638, 114479.

Harnack, D., Kupsch, A., 2010. The impact of subthalamic deep brain stimulation on nigral neuroprotection-myth or reality? Neuromodulation 13, 160–167.

Hirsch, E.C., Perier, C., Orieux, G., Francois, C., Feger, J., Yelnik, J., Vila, M., Levy, R., Tolosa, E.S., Marin, C., Trinidad Herrero, M., Obeso, J.A., Agid, Y., 2000. Metabolic effects of nigrostriatal denervation in basal ganglia. Trends Neurosci. 23, S78–S85.
Huang, W.S., Lin, S.Z., Lin, J.C., Wey, S.P., Ting, G., Liu, R.S., 2001. Evaluation of early-stage Parkinson's disease with 99mTc-TRODAT-1 imaging. J. Nucl. Med. 42, 1303–1308.
Iovino, L., Giusti, V., Pischedda, F., Giusto, E., Plotegher, N., Marte, A., Battisti, I., Di Iacovo, A., Marku, A., Piccoli, G., Bandopadhyay, R., Perego, C., Bonifacino, T., Bonanno, G., Roseti, C., Bossi, E., Arrigoni, G., Bubacco, L., Greggio, E., Hilfiker, S., Civiero, L., 2022. Trafficking of the glutamate transporter is impaired in LRRK2-related Parkinson's disease. Acta Neuropathol. 144, 81–106.
Iravani, M.M., McCreary, A.C., Jenner, P., 2012. Striatal plasticity in Parkinson's disease and L-dopa induced dyskinesia. Parkinsonism Relat. Disord. 18 (Suppl. 1), S123–S125.
Jiang, Z.G., North, R.A., 1991. Membrane properties and synaptic responses of rat striatal neurones in vitro. J. Physiol. 443, 533–553.
Klietz, M., Bronzlik, P., Nosel, P., Wegner, F., Dressler, D.W., Dadak, M., Maudsley, A.A., Sheriff, S., Lanfermann, H., Ding, X.Q., 2019. Altered neurometabolic profile in early Parkinson's disease: a study with short Echo-time whole brain MR spectroscopic imaging. Front. Neurol. 10, 777.
Le Fur, Y., Nicoli, F., Guye, M., Confort-Gouny, S., Cozzone, P.J., Kober, F., 2010. Grid-free interactive and automated data processing for MR chemical shift imaging data. MAGMA 23, 23–30.
Li, P., Ensink, E., Lang, S., Marshall, L., Schilthuis, M., Lamp, J., Vega, I., Labrie, V., 2020. Hemispheric asymmetry in the human brain and in Parkinson's disease is linked to divergent epigenetic patterns in neurons. Genome Biol. 21, 61.
Li, X., Wang, W., Yan, J., Zeng, F., 2021. Glutamic acid transporters: targets for neuroprotective therapies in Parkinson's disease. Front. Neurosci. 15, 678154.
Limousin, P., Pollak, P., Benazzouz, A., Hoffmann, D., Broussolle, E., Perret, J.E., Benabid, A.L., 1995. Bilateral subthalamic nucleus stimulation for severe Parkinson's disease. Mov. Disord. 10, 672–674.
Lovinger, D.M., 2010. Neurotransmitter roles in synaptic modulation, plasticity and learning in the dorsal striatum. Neuropharmacology 58, 951–961.
Lovinger, D.M., Tyler, E.C., Merritt, A., 1993. Short- and long-term synaptic depression in rat neostriatum. J. Neurophysiol. 70, 1937–1949.
Madeo, G., Martella, G., Schirinzi, T., Ponterio, G., Shen, J., Bonsi, P., Pisani, A., 2012. Aberrant striatal synaptic plasticity in monogenic parkinsonisms. Neuroscience 211, 126–135.
Magi, S., Piccirillo, S., Amoroso, S., Lariccia, V., 2019. Excitatory amino acid transporters (EAATs): glutamate transport and beyond. Int. J. Mol. Sci. 20.
Marek, K.L., Seibyl, J.P., Zoghbi, S.S., Zea-Ponce, Y., Baldwin, R.M., Fussell, B., Charney, D.S., van Dyck, C., Hoffer, P.B., Innis, R.P., 1996. [123I] beta-CIT/SPECT imaging demonstrates bilateral loss of dopamine transporters in hemi-Parkinson's disease. Neurology 46, 231–237.
Maudsley, A.A., Andronesi, O.C., Barker, P.B., Bizzi, A., Bogner, W., Henning, A., Nelson, S.J., Posse, S., Shungu, D.C., Soher, B.J., 2021. Advanced magnetic resonance spectroscopic neuroimaging: Experts' consensus recommendations. NMR Biomed. 34, e4309.
McKinnon, C., Gros, P., Lee, D.J., Hamani, C., Lozano, A.M., Kalia, L.V., Kalia, S.K., 2019. Deep brain stimulation: potential for neuroprotection. Ann. Clin. Transl. Neurol. 6, 174–185.
Melon, C., Chassain, C., Bielicki, G., Renou, J.P., Kerkerian-Le Goff, L., Salin, P., Durif, F., 2015. Progressive brain metabolic changes under deep brain stimulation of subthalamic nucleus in parkinsonian rats. J. Neurochem. 132, 703–712.
Meyerspeer, M., Scheenen, T., Schmid, A.I., Mandl, T., Unger, E., Moser, E., 2011. Semi-LASER localized dynamic 31P magnetic resonance spectroscopy in exercising muscle at ultra-high magnetic field. Magn. Reson. Med. 65, 1207–1215.
Michel, P.P., Hirsch, E.C., Hunot, S., 2016. Understanding dopaminergic cell death pathways in Parkinson disease. Neuron 90, 675–691.
Muddapu, V.R., Mandali, A., Chakravarthy, V.S., Ramaswamy, S., 2019. A computational model of loss of dopaminergic cells in Parkinson's disease due to glutamate-induced excitotoxicity. Front. Neural Circ. 13, 11.
Nafia, I., Re, D.B., Masmejean, F., Melon, C., Kachidian, P., Kerkerian-Le Goff, L., Nieoullon, A., Had-Aissouni, L., 2008. Preferential vulnerability of mesencephalic dopamine neurons to glutamate transporter dysfunction. J. Neurochem. 105, 484–496.
Olanow, C.W., 2007. The pathogenesis of cell death in Parkinson's disease–2007. Mov. Disord. 22 (Suppl. 17), S335–S342.
Pagano, G., Ferrara, N., Brooks, D.J., Pavese, N., 2016. Age at onset and Parkinson disease phenotype. Neurology 86, 1400–1407.
Paille, V., Picconi, B., Bagetta, V., Ghiglieri, V., Sgobio, C., Di Filippo, M., Viscomi, M.T., Giampa, C., Fusco, F.R., Gardoni, F., Bernardi, G., Greengard, P., Di Luca, M., Calabresi, P., 2010. Distinct levels of dopamine denervation differentially alter striatal synaptic plasticity and NMDA receptor subunit composition. J. Neurosci. 30, 14182–14193.
Partridge, J.G., Tang, K.C., Lovinger, D.M., 2000. Regional and postnatal heterogeneity of activity-dependent long-term changes in synaptic efficacy in the dorsal striatum. J. Neurophysiol. 84, 1422–1429.
Patterson, J.R., Duffy, M.F., Kemp, C.J., Howe, J.W., Collier, T.J., Stoll, A.C., Miller, K. M., Patel, P., Levine, N., Moore, D.J., Luk, K.C., Fleming, S.M., Kanaan, N.M., Paumier, K.L., El-Agnaf, O.M.A., Sortwell, C.E., 2019. Time course and magnitude of alpha-synuclein inclusion formation and nigrostriatal degeneration in the rat model of synucleinopathy triggered by intrastriatal alpha-synuclein preformed fibrils. Neurobiol. Dis. 130, 104525.
Pawlak, V., Kerr, J.N., 2008. Dopamine receptor activation is required for corticostriatal spike-timing-dependent plasticity. J. Neurosci. 28, 2435–2446.
Paxinos, G., Watson, C., 1998. The Rat Brain in Stereotaxic Coordinates. Academic Press, New York.
Prasad, S., Saini, J., Yadav, R., Pal, P.K., 2018. Motor asymmetry and neuromelanin imaging: concordance in Parkinson's disease. Parkinsonism Relat. Disord. 53, 28–32.
Provencher, S.W., 1993. Estimation of metabolite concentrations from localized in vivo proton NMR spectra. Magn. Reson. Med. 30, 672–679.
Quiroga-Varela, A., Walters, J.R., Brazhnik, E., Marin, C., Obeso, J.A., 2013. What basal ganglia changes underlie the parkinsonian state? The significance of neuronal oscillatory activity. Neurobiol. Dis. 58, 242–248.
Rae, C.D., 2014. A guide to the metabolic pathways and function of metabolites observed in human brain 1H magnetic resonance spectra. Neurochem. Res. 39, 1–36.
Remple, M.S., Bradenham, C.H., Kao, C.C., Charles, P.D., Neimat, J.S., Konrad, P.E., 2011. Subthalamic nucleus neuronal firing rate increases with Parkinson's disease progression. Mov. Disord. 26, 1657–1662.
Riederer, P., Jellinger, K.A., Kolber, P., Hipp, G., Sian-Hulsmann, J., Kruger, R., 2018. Lateralisation in Parkinson disease. Cell Tissue Res. 373, 297–312.
Rodriguez, M.C., Obeso, J.A., Olanow, C.W., 1998. Subthalamic nucleus-mediated excitotoxicity in Parkinson's disease: a target for neuroprotection. Ann. Neurol. 44, S175–S188.
Schapira, A.H., Jenner, P., 2011. Etiology and pathogenesis of Parkinson's disease. Mov. Disord. 26, 1049–1055.
Schapira, A.H.V., Chaudhuri, K.R., Jenner, P., 2017. Non-motor features of Parkinson disease. Nat. Rev. Neurosci. 18, 435–450.
Schirinzi, T., Madeo, G., Martella, G., Maltese, M., Picconi, B., Calabresi, P., Pisani, A., 2016. Early synaptic dysfunction in Parkinson's disease: insights from animal models. Mov. Disord. 31, 802–813.
Shen, W., Flajolet, M., Greengard, P., Surmeier, D.J., 2008. Dichotomous dopaminergic control of striatal synaptic plasticity. Science 321, 848–851.
Stagg, C.J., Bestmann, S., Constantinescu, A.O., Moreno, L.M., Allman, C., Mekle, R., Woolrich, M., Near, J., Johansen-Berg, H., Rothwell, J.C., 2011. Relationship between physiological measures of excitability and levels of glutamate and GABA in the human motor cortex. J. Physiol. 589, 5845–5855.
Tang, K., Low, M.J., Grandy, D.K., Lovinger, D.M., 2001. Dopamine-dependent synaptic plasticity in striatum during in vivo development. Proc. Natl. Acad. Sci. U. S. A. 98, 1255–1260.
Thiele, S.L., Chen, B., Lo, C., Gertler, T.S., Warre, R., Surmeier, J.D., Brotchie, J.M., Nash, J.E., 2014. Selective loss of bi-directional synaptic plasticity in the direct and indirect striatal output pathways accompanies generation of parkinsonism and l-DOPA induced dyskinesia in mouse models. Neurobiol. Dis. 71, 334–344.
Tkac, I., Starcuk, Z., Choi, I.Y., Gruetter, R., 1999. In vivo 1H NMR spectroscopy of rat brain at 1 ms echo time. Magn. Reson. Med. 41, 649–656.
Torres, N., Molet, J., Moro, C., Mitrofanis, J., Benabid, A.L., 2017. Neuroprotective surgical strategies in Parkinson's disease: role of preclinical data. Int. J. Mol. Sci. 18.
Uitti, R.J., Baba, Y., Whaley, N.R., Wszolek, Z.K., Putzke, J.D., 2005. Parkinson disease: handedness predicts asymmetry. Neurology 64, 1925–1930.
van der Hoorn, A., Burger, H., Leenders, K.L., de Jong, B.M., 2012. Handedness correlates with the dominant Parkinson side: a systematic review and meta-analysis. Mov. Disord. 27, 206–210.
Vila, M., Levy, R., Herrero, M.T., Ruberg, M., Faucheux, B., Obeso, J.A., Agid, Y., Hirsch, E.C., 1997. Consequences of nigrostriatal denervation on the functioning of the basal ganglia in human and nonhuman primates: an in situ hybridization study of cytochrome oxidase subunit I mRNA. J. Neurosci. 17, 765–773.
Vila, M., Perier, C., Feger, J., Yelnik, J., Faucheux, B., Ruberg, M., Raisman-Vozari, R., Agid, Y., Hirsch, E.C., 2000. Evolution of changes in neuronal activity in the subthalamic nucleus of rats with unilateral lesion of the substantia nigra assessed by metabolic and electrophysiological measurements. Eur. J. Neurosci. 12, 337–344.
Wang, J., Yang, Q.X., Sun, X., Vesek, J., Mosher, Z., Vasavada, M., Chu, J., Kanekar, S., Shivkumar, V., Venkiteswaran, K., Subramanian, T., 2015. MRI evaluation of asymmetry of nigrostriatal damage in the early stage of early-onset Parkinson's disease. Parkinsonism Relat. Disord. 21, 590–596.
Wiberg, A., Ng, M., Al Omran, Y., Alfaro-Almagro, F., McCarthy, P., Marchini, J., Bennett, D.L., Smith, S., Douaud, G., Furniss, D., 2019. Handedness, language areas and neuropsychiatric diseases: insights from brain imaging and genetics. Brain 142, 2938–2947.
Yagi, S., Yoshikawa, E., Futatsubashi, M., Yokokura, M., Yoshihara, Y., Torizuka, T., Ouchi, Y., 2010. Progression from unilateral to bilateral parkinsonism in early Parkinson disease: implication of mesocortical dopamine dysfunction by PET. J. Nucl. Med. 51, 1250–1257.
Yuksel, C., Ongur, D., 2010. Magnetic resonance spectroscopy studies of glutamate-related abnormalities in mood disorders. Biol. Psychiatry 68, 785–794.
Zhang, Y., Tan, F., Xu, P., Qu, S., 2016. Recent advance in the relationship between excitatory amino acid transporters and Parkinson's disease. Neural Plast. 2016, 8941327.
Zhang, Y., Meng, X., Jiao, Z., Liu, Y., Zhang, X., Qu, S., 2020. Generation of a novel mouse model of Parkinson's disease via targeted knockdown of glutamate transporter GLT-1 in the substantia Nigra. ACS Chem. Neurosci. 11, 406–417.